

# Identification and Characterization of the First Cathelicidin from Sea Snakes with Potent Antimicrobial and Anti-inflammatory Activity and Special Mechanism\*

Received for publication, February 2, 2015, and in revised form, May 7, 2015. Published, JBC Papers in Press, May 26, 2015, DOI 10.1074/jbc.M115.642645

Lin Wei<sup>‡1</sup>, Jiuxiang Gao<sup>§1</sup>, Shumin Zhang<sup>¶1</sup>, Sijin Wu<sup>§</sup>, Zeping Xie<sup>¶</sup>, Guiying Ling<sup>||</sup>, Yi-Qun Kuang<sup>\*\*</sup>, Yongliang Yang<sup>§</sup>, Haining Yu<sup>§2</sup>, and Yipeng Wang<sup>‡‡3</sup>

From the <sup>‡‡</sup>Department of Pharmaceutical Sciences, College of Pharmaceutical Sciences, Soochow University, Suzhou, Jiangsu 215123, China, the <sup>§</sup>Department of Bioscience and Biotechnology, Dalian University of Technology, Dalian, Liaoning 116023, China, the <sup>¶</sup>Binzhou Medical University of Pharmaceutical College, Yantai, Shandong 264003, China, the <sup>‡</sup>Jiangsu Key Laboratory of Infection and Immunity, Institutes of Biology and Medical Sciences, Soochow University, Suzhou, Jiangsu 215123, China, the <sup>||</sup>Cancer Immunology and Immunotherapy Center, Affiliated Hospital of Guiyang Medical College, Guiyang, Guizhou 550004, China, and the <sup>\*\*</sup>Center for Translational Medicine, Huaihe Clinical Institute, Henan University, Kaifeng, Henan 475000, China

**Background:** Cathelicidins are a family of vertebrate antimicrobial peptides that play pivotal roles in host immune defense against microbial invasions.

**Results:** A novel cathelicidin (Hc-CATH) with potent antimicrobial and anti-inflammatory activity and a special mechanism was identified from the sea snake *Hydrophis cyanocinctus*.

**Conclusion:** Hc-CATH is a potent candidate for the development of peptide antibiotics.

**Significance:** Hc-CATH is the first cathelicidin identified from sea snakes and possesses a special anti-inflammatory mechanism.

Cathelicidins are a family of gene-encoded peptide effectors of innate immunity found exclusively in vertebrates. They play pivotal roles in host immune defense against microbial invasions. Dozens of cathelicidins have been identified from several vertebrate species. However, no cathelicidin from marine reptiles has been characterized previously. Here we report the identification and characterization of a novel cathelicidin (Hc-CATH) from the sea snake *Hydrophis cyanocinctus*. Hc-CATH is composed of 30 amino acids, and the sequence is KFFKRLKSVRRRAVKKFRKKPRLIGLSTLL. Circular dichroism spectroscopy and structure modeling analysis indicated that Hc-CATH mainly assumes an amphipathic  $\alpha$ -helical conformation in bacterial membrane-mimetic solutions. It possesses potent broad-spectrum and rapid antimicrobial activity. Meanwhile, it is highly stable and shows low cytotoxicity toward mammalian cells. The microbial killing activity of Hc-CATH is executed through the disruption of cell membrane and lysis of bacterial cells. In addition, Hc-CATH exhibited potent anti-inflammatory activity by inhibiting the LPS-induced production of nitric oxide (NO) and pro-inflammatory cytokines such as TNF- $\alpha$ , IL-1 $\beta$ , and IL-6. Hc-CATH directly binds with LPS to neutralize its toxicity, and it also binds to Toll-like receptor 4

(TLR4/MD2 complex), which therefore inhibits the binding of LPS to TLR4/MD2 complex and the subsequent activation of LPS-induced inflammatory response pathways. Taken together, our study demonstrates that Hc-CATH, the first cathelicidin from sea snake discovered to have both antimicrobial and anti-inflammatory activity, is a potent candidate for the development of peptide antibiotics.

Living in an environment surrounded by diverse microorganisms, multicellular organisms are constantly threatened by the invasion of microbial pathogens (1). The discovery of antibiotics has been one of the greatest achievements of modern medicine, and their widespread use has saved countless patients from lethal infections (2). However, the excessive use of antibiotics has simultaneously prompted the evolution of microbial pathogens, resulting in a large-scale emergence of drug-resistant pathogens such as methicillin-resistant *Staphylococcus aureus* and vancomycin-resistant *Enterococcus*. Meanwhile, rate of development for novel antimicrobial drugs have been declining (3). The human immune system is composed of two branches, innate and adaptive immunity. Innate immunity is the first line of host defense against microbial infection (4, 5). Innate immunity recognizes invading pathogens via germ line-encoded pattern recognition receptors, activates specific signaling pathways such as TLRs<sup>4</sup> and NOD-like receptors, and ultimately leads to the generation of local inflammation at the

\* This work was supported by Grants 41206153 and 81402830 from the Chinese National Natural Science Foundation, SYN201407 from the Suzhou Science and Technology Development Project, BK20140362 and 14KJ350003 from the Jiangsu Province Natural Science Foundation, LQ2013010 from the Growth Project for Liaoning Distinguished Young Scientists of Colleges and Universities, and 2013J21DW013 from the Dalian Distinguished Young Scientists Funding. The authors declare that they have no conflicts of interest with the contents of this article.

<sup>1</sup> These authors made equal contributions to this work.

<sup>2</sup> To whom correspondence may be addressed. Tel.: 86-411-84708850; Fax: 86-411-84708850; E-mail: yuhaining@dlut.edu.cn.

<sup>3</sup> To whom correspondence may be addressed. Tel.: 86-512-65882370; Fax: 86-512-65882370; E-mail: yipengwang@suda.edu.cn.

<sup>4</sup> The abbreviations used are: TLR, toll-like receptor; AMP, antimicrobial peptide; MPM, mouse peritoneal macrophage; qRT-PCR, quantitative real-time PCR; MST, microscale thermophoresis; MIC, minimal inhibitory concentration; Hc-CATH, cathelicidin from *Hydrophis cyanocinctus*; Tricine, N-[2-hydroxy-1,1-bis(hydroxymethyl)ethyl]glycine; PE-TLR4, phycoerythrin-TLR4; MTT, 3-(4,5-dimethyl-2-thiazolyl)-2,5-diphenyl-2-H-tetrazolium bromide; iNOS, inducible nitric-oxide synthase; LAL, limulus amoebocyte lysate.

## The First Cathelicidin from Sea Snakes

site of pathogenic infection (4, 5). Local inflammation plays an important role in the early stage of invading pathogen eradication. Therefore, modulation of innate immunity is regarded as an attractive approach to anti-infective therapy for its potential broader applications and the slight possibility of inducing microbial resistance (6–8). However, hyperactivation of the innate immunity may lead to excessive production of pro-inflammatory cytokines and sepsis, which cause massive damage to the host and even death (6, 7).

Antimicrobial peptides (AMPs) are a large group of gene-encoded small peptides that have been identified in nearly all species of life and play critical roles in host innate immune response to microbial infections (1, 9). They are diverse in sequence and structure and can be divided broadly into several classes (10). However, they are generally amphipathic (containing hydrophobic and hydrophilic patches on the surface) and positively charged (rich in lysine and arginine residues) (10, 11). AMPs typically have broad-spectrum antimicrobial activity against bacteria, fungi, enveloped viruses, and even parasites (10, 11). Besides direct antimicrobial activity, many AMPs also exhibit a variety of other functions, such as chemoattraction of immune cells, neutralization of LPS, wound healing promotion, and induction of angiogenesis (12, 13). Therefore, in recent years AMPs have also been referred to as cationic host defense peptides, which more specifically refers to their multifunctional activities (14). Two major families of AMPs exist in vertebrates, namely defensins and cathelicidins. Whereas defensins are generally characterized by a common  $\beta$ -sheet core structure stabilized by three well defined disulfide bonds (15), the structures of cathelicidins are highly heterogeneous (16). However, cathelicidin precursors share a highly conserved signal peptide and “cathelin” domain at the N terminus. Consistent with other AMPs, most cathelicidins have direct killing activity against a wide range of microorganisms and are actively involved in various phases of host immunity modulation and disease resistance (16, 17). Moreover, their microbial killing and immune modulating activities are more potent than most of the other AMPs characterized thus far. Because of their small size, low toxicity, high stability, and diverse mechanisms, they are deemed attractive candidates for anti-infective agent development (18, 19). There are three cathelicidin analogs being tested in clinical trials: Isegran, Omiganan, and MBI 594AN (20).

To date, nine cathelicidins have been identified from terrestrial snakes, most of which exhibited potent antimicrobial activities (21–23). However, no cathelicidin has been identified from sea snakes. To verify the existence of cathelicidins in sea snakes and to discover more templates for peptide antibiotic design, we report the identification and characterization of a novel cathelicidin (Hc-CATH) from the sea snake *Hydrophis cyanocinctus* in this study. We show that Hc-CATH possesses potent broad-spectrum and rapid antimicrobial activity, high stability, low cytotoxicity, and strong anti-inflammatory activity, all of which make it a potent candidate for the development of novel peptide antibiotics.

### Experimental Procedures

**Sea Snake Collection and Tissue Preparation**—Adult specimens of *H. cyanocinctus* ( $n = 2$ , female, weight range 200–350 g) were

collected from Beihai, Guangxi Province, China (21.482°N, 109.119°E). After collection, the snakes were killed, and the venom glands, spleen, lung, skin, and muscle were dissected immediately and frozen in liquid nitrogen until used. No specific permissions were required for the sampling location/activity, and the present study did not involve endangered or protected species. The animal experimental protocol in the present study was approved by the Animal Care and Use Ethics Committee of Soochow University.

**cDNA Synthesis and Screening of Genes Encoding Cathelicidin**—Total RNA of the snake venom glands ( $n = 2$ , weight range 0.35 to 0.5 g) was extracted using TRIzol reagent (Life Technologies, Inc.) in accordance with the manufacturer's instructions. cDNA synthesis was carried out by a PCR-based method using an In-Fusion SMARTer™ directional cDNA library construction kit (Clontech, Palo Alto, CA). First-strand cDNA was synthesized by SMARTScribe™ reverse transcriptase (Clontech), and the primers used were SMARTer V oligonucleotide (5'-AAGCAGTGGTATCAACGCAGAGTAXX-XXX-3', where X = undisclosed base in the proprietary SMARTer oligo sequence) and 3'-IF SMARTer CDS primer (5'-CGGGGTACGATGAGACACCATTTTTTTTTTTTTTTT-TTTTTTVN-3', where N = A, C, G, or T and V = A, G, or C) supplied by the kit. Second-strand cDNA was amplified by a long-distance PCR method using Advantage 2 polymerase mix supplied by the kit, and the primers used were 5'-PCR Primer IIA (5'-AAGCAGTGGTATCAACGCAGAGT) and 3'-IF SMARTer PCR primer (5'-CGGGGTACGATGAGACACCA-3'). The synthesized second-strand cDNAs were used as templates for the PCR-based cDNA screening described below.

According to the highly conserved cathelin domain of previously characterized snake cathelicidins, a 3' antisense primer (5'-CCCCTCCTCCTGCTTCTGCT-3') was designed and coupled with the 5' sense primer (5'-AAGCAGTGGTATCAACGCAGAGT-3') designed based on the SMARTer V oligonucleotide primer to screen the 5' fragments of cDNAs encoding the cathelicidins of *H. cyanocinctus*. The PCR procedure was as follows: 5 min of denaturation at 94 °C, 30 cycles of denaturation at 94 °C for 30 s, primer annealing at 58 °C for 30 s, and extension at 72 °C for 1 min. The last cycle was followed by an extension step at 72 °C for 10 min. The PCR product was purified by gel electrophoresis and cloned into pMD19-T vector (Takara, Japan) for sequencing.

After the 5' fragments of cDNAs were obtained, a sense primer (5'-GAGGATGCAAGGGTTCTTCTGG-3') was designed according to the 5' coding region and coupled with the 3' antisense primer (5'-TACGCGACGCGATACGCGAA-T-3'), designed based on the sequence of 3'-IF SMARTer CDS primer to screen the full-length cDNAs. The PCR procedure was as follows: 5 min at 94 °C and 30 cycles of 30 s at 94 °C, 30 s at 56 °C, and 60 s at 72 °C. The last cycle was followed by an extension step at 72 °C for 10 min. The PCR product was also purified by gel electrophoresis and cloned into pMD19-T vector (Takara, Japan) for sequencing.

**Multi-sequence Alignment and Phylogenetic Analysis**—The cathelicidin sequences used for multi-sequence alignment and phylogenetic analysis were obtained from the protein database at the National Center for Biotechnology Information (NCBI).

**TABLE 1**  
Physicochemical parameters of Hc-CATH and its derivatives

Peptide	Sequence	Net charge	Theoretical pI	$M_r$
Hc-CATH	KFFKRLKSVRRRAVKKFRKKPRLIGLSTLL	+12	12.61	3628.5
Hc-CATH1	KFFARLLASVRAAVKKFRKKPRLIGLSTLL	+9	12.49	3429.2
Hc-CATH2	AFFARLLASVRAAVKFAKPPRLIGLSTLL	+6	12.31	3229.9
sHc-CATH	LKKLKGVRVSRSLFFVVKLRPAKRTLKRRIL	+12	12.61	3628.5

Multi-sequence alignment was carried out using Clustal 2.1 and GeneDoc software. The phylogenetic tree was constructed by the Neighbor-joining algorithm using the MEGA program (version 5.0). To avoid the mistakes caused by the diversity of mature peptides, we used the conserved signal peptide and cathelin domain to construct the phylogenetic tree. A total of 1000 bootstrap replicates were used to test the reliability of each branch. The numbers on the branches indicate the percentage of 1000 bootstrap samples supporting the branch (Fig. 3).

**Bioinformatic Analysis and Structure Modeling**—The physical and chemical parameters of Hc-CATH were analyzed by using the ExPASy Bioinformatics Resource Portal. The secondary structure of Hc-CATH was predicted by The PSIPRED (Protein Structure Prediction) server provided by the Bioinformatics Group of the Department of Computer Science, University College London. The helix-wheel plot was constructed using the software package provided by the Expert Protein Analysis System (ExPASy) proteomics server. Structure modeling of Hc-CATH was conducted using a *de novo* design modeling method. Hc-CATH was searched and aligned in BLAST. The Rosetta *ab initio* protocol was used to predict the three-dimensional structure of Hc-CATH. 5000 decoys were obtained from the Rosetta *ab initio* prediction result. After clustering, the lowest energy structure of Hc-CATH was verified by PROCHECK. The three-dimensional structure generated was visualized by using PyMOL software without any refinement.

**Peptide Synthesis**—Hc-CATH and its derivatives, isotype control sHc-CATH and FITC-labeled peptides (FITC conjugates to the N terminus of Hc-CATH and sHc-CATH), were synthesized by the peptide synthesizer GL Biochem Ltd. (Shanghai, China). Their physicochemical parameters are shown in Table 1. The synthetic peptides were purified and then analyzed by HPLC and MALDI-TOF MS to confirm that the purity was higher than 98%.

**Native Hc-CATH Confirmation Analysis**—The synthetic Hc-CATH was used as the antigen to immunize C57 mice. The mouse serum was collected, and the polyclonal antibody of Hc-CATH was purified using CNBr-activated Sepharose 4B (GE Healthcare) in accordance with the manufacturer's instructions. Several tissues including venom gland, spleen, lung, skin, and muscle were randomly selected, total proteins from which were extracted and separated by Tricine-SDS-PAGE. Western blot was performed using the prepared mouse Hc-CATH polyclonal antibody. A primary monoclonal antibody of mouse  $\beta$ -actin (GoodScience Biotech Co., Shanghai, China) was used as a control.

**Circular Dichroism Spectroscopy**—Circular dichroism (CD) spectroscopy was used to evaluate the secondary structure of Hc-CATH in solvent environments. The CD spectra were recorded at 298 K on a Jasco J-715 spectrophotometer (Jasco). Samples were prepared by dissolving Hc-CATH to an ultimate

concentration of 0.2 mg/ml in SDS/H<sub>2</sub>O solutions of different concentrations (0, 30, 60, 90, and 120 mM). Spectra at 190–260 nm were measured; the instrument parameters were: 0.1 cm path-length cell, 1 nm bandwidth, 1 s response time, and a scan speed of 100 nm/min. For each sample, three consecutive scans were performed and averaged followed by subtraction of the solvent signal.

To investigate the effect of salt and temperature on the structure of Hc-CATH, the secondary structures of Hc-CATH in NaCl solutions and at high temperatures were determined by CD spectroscopy. For the salt assay, Hc-CATH was dissolved in 60 mM SDS/H<sub>2</sub>O solution with serial concentrations of NaCl (0, 100, 200, and 400 mM) to an ultimate concentration of 0.2 mg/ml, and the CD spectra of these samples were measured. For the temperature assay, Hc-CATH was dissolved in 60 mM SDS/H<sub>2</sub>O solution to an ultimate concentration of 0.2 mg/ml. The samples were incubated at different temperatures (20, 50, 70, and 90 °C) for 1 h, and then the CD spectra were recorded.

**Antimicrobial Assay**—To determine the antimicrobial potency of Hc-CATH, a 2-fold broth microdilution method was used as described in our previous work (24). 48 human pathogenic microbial strains (26 Gram-negative bacteria, 12 Gram-positive bacteria, and 10 fungi) were used in the present assay, in which the standard strains were stored in our laboratory and the clinical strains were collected from local hospitals. Briefly, microbes were incubated in Mueller-Hinton broth (MH broth) at 37 °C to exponential phase and diluted to 10<sup>6</sup> cfu/ml. A serial dilution of Hc-CATH was prepared in 96-well microtiter plates (50  $\mu$ l) and mixed with equal volume of microbial inoculums (50  $\mu$ l). The plates were put into a microbial incubator and shaken slowly (100 rpm) at 37 °C for 18 h. At the terminal point of incubation, the plates were put into an ELISA plate reader, and the growth of the microbe was determined by measuring the absorbance values (A) at 600 nm. The minimal concentrations at which no microbial growth occurred were recorded as MIC values. Two traditional antibiotics (ampicillin and meropenem) were used as positive controls.

To determine the antimicrobial activity of Hc-CATH toward pathogens of sea snakes, 11 marine aquatic pathogenic bacteria were collected, and their sensitivity to Hc-CATH was determined. The bacteria were cultured in nutrient broth (Thermo Scientific), and the above described 2-fold broth microdilution method was used to determine the MIC values.

**Bacterial Killing Kinetic Assay**—The bacterial killing kinetic assay was carried out according to the method described previously with minor modifications (22). *Escherichia coli* ATCC25922 was incubated in MH broth to exponential phase and diluted to 10<sup>6</sup> cfu/ml with fresh MH broth. Hc-CATH was added to the bacterial suspension to a final concentration of 5  $\times$  MIC (11.7  $\mu$ g/ml), and the bacteria were incubated at

## The First Cathelicidin from Sea Snakes

37 °C for 0, 10, 20, 30, 45, 60, 90, 120, and 180 min. At each time point, 50- $\mu$ l aliquots were extracted and diluted with fresh MH broth for 1000 times, and 50  $\mu$ l of the dilution was coated on MH agar plates. The plates were incubated at 37 °C for 18 h, and the viable colonies were counted. Meropenem and sterile deionized water were used as the positive and blank control, respectively.

**Salt Tolerance, Thermal Tolerance, Thermal Stability, and Serum Stability**—Salt tolerance of Hc-CATH was examined as described previously (25). Briefly, *E. coli* ATCC25922 was incubated in MH broth to exponential phase and diluted to 10<sup>6</sup> cfu/ml in fresh MH broth with sodium chloride at final concentrations of 0, 50, 100, 150, 200 and 400 mM, respectively. Serial dilutions of Hc-CATH prepared with the same MH broth were added to the *E. coli* ATCC25922 suspension. The bacteria were incubated at 37 °C for 18 h, and the MIC values of Hc-CATH against *E. coli* ATCC25922 in the presence of different concentrations of sodium chloride were determined.

Thermal tolerance of Hc-CATH was determined by measuring MIC values of Hc-CATH against *E. coli* ATCC25922 after incubated at different temperatures. The experiment was carried out as previously described (25). Briefly, Hc-CATH was dissolved in sterile deionized water to an ultimate concentration of 2 mg/ml and incubated at different temperatures (4, 20, 37, 50, 70, and 90 °C) for 1 h. After that, the MICs of the peptide solutions against *E. coli* ATCC25922 were determined.

The thermal stability of Hc-CATH was examined according to the method described in our previous work (25). Hc-CATH was dissolved in sterile deionized water to an ultimate concentration of 2 mg/ml. The peptide solution was incubated at 37 °C for 0–96 h. At each time point, the MICs of Hc-CATH against *E. coli* ATCC25922 were determined.

The serum stability assay was carried out to evaluate the effect of serum on the antimicrobial activity of Hc-CATH. Briefly, Hc-CATH was dissolved in sterile deionized water to an ultimate concentration of 10 mg/ml. Human serum was mixed with Hc-CATH solution in a volume ratio of 4:1 to confirm that the volume percentage of human serum accounted for 80% of the mixture; the ultimate concentration of Hc-CATH was 2 mg/ml. The mixture was incubated at 37 °C for 0–6 h, and at each time point, aliquots were taken and the MICs against *E. coli* ATCC25922 were determined.

**Cytotoxic and Hemolytic Assay**—The cytotoxic activity of Hc-CATH was determined using the MTT (Sigma) method. Two mammalian tumor cell lines (human liver hepatocellular carcinoma cell line HepG2 and human prostate cancer cell line PC3), one normal mammalian cell line (mice fibroblast cell line L929), and mouse peritoneal macrophages were used for the assay, and the experiment was carried out as described in our previous work (25). Briefly, the cells were cultured in DMEM supplemented with 10% fetal bovine serum in a humidified 5% CO<sub>2</sub> atmosphere at 37 °C. After digestion with trypsin, the cells were diluted with serum-free DMEM to an ultimate concentration of  $\sim 2 \times 10^5$  cells/ml. The cells were seeded in 96-well plates (100  $\mu$ l/well) and cultured overnight until adhesion. Hc-CATH dissolved in serum-free DMEM was added to wells, and the plates were incubated at 37 °C for 48 h. The subsequent procedure was performed according to the standard MTT method.

Cell death induced by Hc-CATH was expressed as the percentage of the negative control group, which was regarded as 100%.

To evaluate the cytotoxic activity of Hc-CATH toward human erythrocytes, hemolytic assay was performed according to the method described in our previous work (25). 1% Triton X-100 (v/v) was used to determine 100% hemolysis, and 0.9% saline was used as negative control. The hemolytic rates of Hc-CATH at different concentrations were recorded.

**Scanning Electron Microscopy (SEM)**—To examine the cellular morphology alteration induced by Hc-CATH, an SEM experiment was performed as described previously (26). Briefly, *S. aureus* ATCC25923 and *E. coli* ATCC25922 were cultured in MH broth to exponential phase, washed with 0.15 M sodium chloride solution three times, and resuspended. Hc-CATH was added to the bacterial suspension to an ultimate concentration of 5 $\times$  MIC and incubated at 37 °C for 30 min. After centrifuged at 1000 rpm for 10 min, the bacterial pellets were fixed with 2.5% glutaraldehyde solution at 4 °C for 2 h, postfixed in 1% osmium tetroxide for 2 h, dehydrated in a graded series of ethanol, frozen in liquid nitrogen-cooled tertbutyl alcohol, vacuum-dried overnight, mounted onto aluminum stubs, and vacuum sputter-coated with gold. Finally, the prepared samples were observed with a Hitachi S-4800 SEM (Japan) under standard operating conditions.

**NO Detection**—Brewer thioglycollate medium (Sigma-Aldrich) was injected into the peritoneal cavity of C57 mice. 3 days later, the mice were euthanized, and peritoneal macrophages were harvested (27). MPM cells were cultured in RPMI 1640 (containing 10% FBS, 100 units/ml penicillin, and 100  $\mu$ g/ml streptomycin; Gibco) and plated in 96-well culture plate ( $1 \times 10^4$  cells/well). After adhesion, the medium was replaced with fresh RPMI 1640 (containing 2% FBS, 100 units/ml penicillin, and 100  $\mu$ g/ml streptomycin). The cells were co-incubated with LPS (100 ng/ml, from *E. coli* 055:B5, Sigma-Aldrich) and Hc-CATH (0, 1, 2, and 4  $\mu$ g/ml) or preincubated with Hc-CATH (0, 1, 2, and 4  $\mu$ g/ml) for 30 min, washed twice with PBS buffer to remove the peptide, and then stimulated with LPS (100 ng/ml) for 24 h. The cells were centrifuged, and the culture medium was harvested to detect NO production. NO production was determined by detecting the nitrite level using Griess reagent (Beyotime, Shanghai, China) according to the manufacturer's instructions. The effects of sHc-CATH and Hc-CATH1 and -2 on NO production induced by LPS were also determined. MPM cells were co-incubated with LPS (100 ng/ml) and peptides (4  $\mu$ g/ml) for 24 h, and then the NO production in the culture supernatant was determined.

**Quantitative Real-time PCR**—MPM cells were co-incubated with Hc-CATH (0, 1, 2, and 4  $\mu$ g/ml) and LPS (100 ng/ml) or preincubated with Hc-CATH (0, 1, 2, and 4  $\mu$ g/ml) for 30 min before LPS (100 ng/ml) stimulation as described under "NO Detection" above. After treatment for 6 h, the cells were collected for quantitative real-time PCR (qRT-PCR) to examine the gene expression level of iNOS and pro-inflammatory cytokines TNF- $\alpha$ , IL-1 $\beta$ , and IL-6. Briefly, total RNA was isolated using TRIzol reagent (Life Technologies). cDNA was synthesized using the PrimeScript 1st Strand cDNA synthesis kit (Takara, Japan), and qRT-PCR was performed using the SYBR Premix Ex Taq<sup>TM</sup> II (Tli RNaseH Plus) two-step qRT-PCR kit

**TABLE 2**  
Primers (mouse) used for qRT-PCR

Name	Forward	Reverse
	5'-3'	3'-5'
TNF- $\alpha$	CGGTGCCTATGTCCTCAGCCT	GAGGTCTGGCCATAGAAC
IL-1 $\beta$	ATGGCAACTGTTCCTGAACTC	GCCCATACTTTAGGAAGACA
iNOS	CTGCAGCACTTGGATCAGGAACCTG	GGAGTAGCCTGTGTGCACCTGGAA
IL-6	AGTTGCCTTCTTGGACTGA	TCCACGATTTCCAGAGAAC
GAPDH	GTGAAGTTCGGTGTGACCGATT	GGAGATGATGACCTTTTGGCTC

(Takara Bio Inc., Shiga, Japan) on an ABI Prism 7000 real-time PCR system (Applied Biosystems, Carlsbad, CA). The cycle counts of the target genes were normalized to the GAPDH gene, and accordingly the fold changes of the target genes were calculated. The primers used for qRT-PCR are listed in Table 2.

**Pro-inflammatory Cytokine Determination**—MPMs were co-incubated with Hc-CATH (0, 1, 2, and 4  $\mu$ g/ml) and LPS (100 ng/ml) or preincubated with Hc-CATH (0, 1, 2, and 4  $\mu$ g/ml) for 30 min before LPS (100 ng/ml) stimulation as described under “NO Detection” above. After 6 h, the cell culture supernatants were collected and assessed for TNF- $\alpha$ , IL-1 $\beta$ , and IL-6 by ELISA (eBiosciences). The effects of sHc-CATH and Hc-CATH1 and -2 on LPS-induced pro-inflammatory cytokine production were also determined. MPM cells were co-incubated with LPS (100 ng/ml) and peptides (4  $\mu$ g/ml) for 6 h, and the pro-inflammatory cytokines in the culture supernatant were determined.

**Western Blot Analysis**—MPM cells were cultured in 6-well plate with RPMI 1640 (2% FBS). The cells were co-incubated with LPS (100 ng/ml) and Hc-CATH (2  $\mu$ g/ml) or preincubated with Hc-CATH (2  $\mu$ g/ml) for 15 min before the addition of LPS (100 ng/ml). After incubation for 30 min, the cells were collected and washed twice with ice-cold PBS, and then the cytoplasmic or nuclear proteins were extracted for Western blot analysis according to our previously described method (28). Primary antibodies of phospho-ERK/ERK, phospho-JNK/JNK, phospho-p38/p38, NF- $\kappa$ B p65 (1:2000, Cell Signaling Technology), and GAPDH (1:2000, Dingguo Biotech) were used in Western blot analysis.

**LPS Binding and Neutralization Assay**—To examine the binding of LPS to Hc-CATH, microscale thermophoresis (MST) was performed using a Monolith NT.115 instrument (Nano Temper Technologies GmbH). FITC-conjugated LPS from *E. coli* 0111:B4 (FITC-LPS, Sigma-Aldrich) was dissolved in 0.01 M PBS buffer to a constant concentration of 6.75  $\mu$ M. The non-labeled Hc-CATH was diluted with 0.01 M PBS buffer in a dilution series with the highest concentration at 275  $\mu$ M. 10  $\mu$ l of the different Hc-CATH dilutions were mixed with 10  $\mu$ l of the FITC-LPS solutions. Mixed samples were loaded into glass capillaries, and the MST analysis was performed. The MST curves were fitted with a Hill method using Origin version 8.5 software to obtain a  $K_d$  value for binding between FITC-LPS and Hc-CATH.

The ability of Hc-CATH to neutralize LPS was measured using a quantitative chromogenic limulus amoebocyte lysate (LAL) method with a ToxinSensor<sup>TM</sup> chromogenic LAL endotoxin assay kit (GenScript, Nanjing, China). The LPS supplied by the kit was dissolved with LAL water to 5 endotoxin units/ml. Stock solutions of peptides (2 mg/ml) were prepared in LAL water. Peptides at serial concentrations were prepared in a

pyrogen-free 96-well microtiter plate (20  $\mu$ l), an equal volume of LPS solution was added to each well, and the mixture was incubated at 37  $^{\circ}$ C for 30 min to allow peptide binding to LPS. 40  $\mu$ l of LAL reagent was added to each well, and the mixture was incubated at 37  $^{\circ}$ C for 10 min. 40  $\mu$ l of chromogenic substrate reagent was added to each well, and the mixture was further incubated at 37  $^{\circ}$ C for 6 min. After that, 40  $\mu$ l of color stabilizer 1, 2, and 3 was added successively, and the absorbance at 545 nm was measured in an ELISA plate reader. The percent LPS neutralization was calculated as  $(A_{\text{blank}} - A_{\text{sample}})/A_{\text{blank}} \times 100$ , where  $A_{\text{blank}}$  represents the absorbance of blank control (20  $\mu$ l of LAL water + 20  $\mu$ l of LPS solution).

**Flow Cytometry Analysis**—To determine the binding of Hc-CATH to the bacterial cells, the bacteria were cultured to exponential phase, washed twice with PBS, incubated with FITC-Hc-CATH or FITC-sHc-CATH (2  $\mu$ g/ml) for 5 min at 37  $^{\circ}$ C, and washed twice with PBS. To evaluate the binding of Hc-CATH to MPM cells, the cells were incubated with FITC-Hc-CATH or FITC-sHc-CATH (2  $\mu$ g/ml) for 15 min at 37  $^{\circ}$ C and washed twice with PBS. To evaluate the binding effect of Hc-CATH on the plasma membrane TLR4 of MPM cells, the cells were preincubated with Hc-CATH (2  $\mu$ g/ml) at 37  $^{\circ}$ C for 15 min. After being washed with PBS for two times, the cells were stained with anti-mouse PE-TLR4 (2  $\mu$ g/ml, BioLegend) for 30 min at 4  $^{\circ}$ C. All of the bacteria and cell samples were finally washed with PBS and measured on a flow cytometer (BD FACSCanto<sup>TM</sup> II, BD Biosciences). Data were analyzed using FlowJo software 7.6.1 (Tree Star Inc.).

**Molecular Docking Study of Hc-CATH and TLR4/MD2 Complex**—A molecular docking experiment was used to predict the interaction of Hc-CATH with the TLR4/MD2 complex and to analyze their binding pattern. The *de novo* design modeling structure of Hc-CATH obtained (see “Bioinformatic Analysis and Structure Modeling” above) was used for the protein-peptide docking study. The crystallographic structure of TLR4/MD2 was obtained from the Protein Data Bank (PDB code: 4G8A). For protein-peptide docking, Zdock 3.0.2 was first employed to obtain the initial complex structure of TLR4/MD2-peptide. 3600 decoy structures were obtained from the Zdock rigid binding prediction, from which the decoy structure with the highest score in the largest cluster was selected for the next step, flexible docking analysis. RosettaDock was used for the flexible docking analysis. 1000 decoy structures were obtained, from which the TLR4/MD2-Hc-CATH complex structure with the lowest interface binding energy score was acquired. The docking structure generated was visualized using PyMOL software.

## Results

**Identification and Characterization of Hc-CATH**—By gene cloning, a cDNA sequence encoding a novel cathelicidin termed Hc-CATH was obtained from the synthesized second-strand cDNAs of the sea snake venom gland (GenBank<sup>TM</sup> accession number KP202856). As shown in Fig. 1A, the cDNA sequence is 732 bp in length, and the translated Hc-CATH precursor comprises 187 amino acid residues. Multi-sequence alignment of Hc-CATH precursor with other representative vertebrate cathelicidins revealed that consistent with other

## The First Cathelicidin from Sea Snakes

**A** atgcaagggttctctggaagaccttctgggtggtgcagctctcaccatcggtgggacc 60  
 M Q G F F W K T L L V V A A L T I G G T 20  
 tctctcctccacacaaaccctgacctatgaggagcgctggaccttgcagtgacate 120  
 S S L P H K P L T Y E E A V D L A V S I 40  
 tacaacagcaaatctagggaagagtctctgtaccgtgtcttgatgctgttctctcacc 180  
 Y N S K S R E E F L Y R V L D A V P P P 60  
 aagtgggatcctcttctgaaagcaacaagagctgaacttcaactatcaaggagacggtg 240  
 K W D P L S E S N Q E L N F T I K E T V 80  
 tgcccggtggccgaagaacggtcttggaggaatgcggttccaggaagacggggcgctc 300  
 C P V A E E R S L E E C G F Q E D G A V 100  
 atgggatgcacagctactttttcttggcagtgcccccgggtggtctcagctc 360  
 M G C T G Y F F F G E S P P V L V L T C 120  
 gagccttgggtgaaagaagcagcagaagcaggaggagggaacaggaggagaaggag 420  
 E P L V E E E Q Q K Q E E G N E E E K E 140  
 gaaaagggaagacgagaagatcagcccaggagggtcaagaggttcaggaaattttc 480  
 E K E E D E K D Q P R R V K R F R **K F F** 160  
 aaaaagctgctgaaagacgctgagcgtgagctcaagaaatcaggaagaagccgagctc 540  
**K R L L K S V R R A V K K F R K K P R L** 180  
 atcgggctctccacctctcttaagagaggactcgaagagaccggcagcctccactctc 600  
**I G L S T L L** \* 187  
 tgatcccagaaaacggtagagaaaatgagccggctgctccagtcagtcagatcattt 660  
 ccgataggatgctctgccaatcaatcatgaataacaatatatactcaaaaaaaa 720  
 aaaaaaaaaa 732

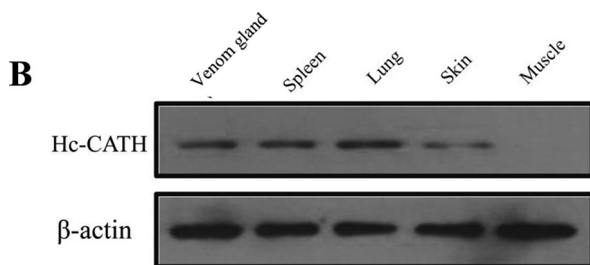


**FIGURE 1. The cDNA sequence encoding Hc-CATH and native Hc-CATH expression in snake tissues.** *A*, the nucleotide sequence encoding Hc-CATH and the deduced amino acid sequence of Hc-CATH precursor. The putative mature peptide is boxed. The stop codon is indicated by an asterisk (\*). *B*, the native Hc-CATH expression in different snake tissues. The synthetic Hc-CATH was used as antigen to immunize mice, and the polyclonal antibody of Hc-CATH was prepared. Western blot was performed using the prepared polyclonal antibody, and  $\beta$ -actin was used as control.

cathelicidins, Hc-CATH precursor is composed of an N-terminal signal peptide sequence, a highly conserved cathelin domain, and a variable C-terminal mature peptide sequence (Fig. 2). Noticeably, the Hc-CATH precursor exhibits a high degree of similarity with the other cathelicidins in the signal and cathelin regions (Fig. 2). Particularly, the four cysteines that are highly conserved at the end of cathelin domain in all cathelicidins are also invariantly spaced in the Hc-CATH precursor. The above results clearly confirm that Hc-CATH is genuinely a novel cathelicidin of sea snake.

Despite high sequence conservation in the signal and cathelin domains, Hc-CATH and the other cathelicidins are drastically diverse in the C-terminal mature region. Previously, a novel cathelicidin termed cathelicidin-BF was purified from the venom of snake *Bungarus fasciatus*, and sequence alignment indicates that Hc-CATH and cathelicidin-BF share conserved cleavage sites for the process of maturation (22). As a result, the mature peptide of Hc-CATH was predicted (Fig. 1A). Hc-CATH is composed of 30 amino acid residues, and the amino acid sequence is KFFKRLKSVRRRAVKKFRKKPRLIGLSTLL. The physicochemical parameters of Hc-CATH are shown in

Table 1. A sequence BLAST with the NCBI protein database indicates that Hc-CATH shows the highest similarity (60%) with cathelicidin-OH from king cobra (23) and a lower identity with those of other vertebrates.

**Evolutionary Analysis of Cathelicidins**—The identification of Hc-CATH provides an opportunity to study the evolutionary relationship of cathelicidins from terrestrial vertebrates and marine vertebrates. Using the neighbor-joining method, we performed the phylogenetic analysis of Hc-CATH together with other representative vertebrate cathelicidins. All cathelicidins generally were divided into five distinct clusters, *i.e.* cathelicidins from fishes, snakes, frogs, birds, and mammals (Fig. 3). Consistent with our prediction, Hc-CATH clustered with the cathelicidins from terrestrial snakes, which implies that Hc-CATH and the cathelicidins from terrestrial snakes originate from a common ancestor. In addition, cathelicidins from elapids and vipers obviously formed two distinct subclusters, and Hc-CATH clustered with elapid cathelicidins, suggesting a closer relationship of Hc-CATH with the elapid cathelicidins.

**Confirmation of the Existence of Native Hc-CATH in Snakes**—To confirm the existence of native Hc-CATH in snakes, we prepared a polyclonal antibody of Hc-CATH and performed Western blot analysis. As shown in Fig. 1B, native Hc-CATH apparently exists in the venom gland, spleen, lung, and skin. Among these, the expression level in the skin was relatively low. However, the expression of Hc-CATH was not detected in muscle.

**Secondary Structure of Hc-CATH**—As shown in Fig. 4A, the main region of Hc-CATH, especially the N-terminal region (Lys-1–Lys-19), was predicted to adopt an  $\alpha$ -helical conformation. Besides, another short  $\alpha$ -helix region in the middle of Hc-CATH (Arg-22–Ser-27) can also be observed. A proline (Pro-21) presents between the two  $\alpha$ -helix regions, which breaks the extension of the helix structures. A helix-wheel diagram of the N-terminal  $\alpha$ -helix region (Lys-1–Lys-19) was plotted using the software package provided by the ExPASy proteomics server to estimate the amphipathicity of Hc-CATH. As shown in Fig. 4B, the hydrophobic amino acids (shown in yellow and gray) are concentrated on one side of the helix, and the hydrophilic amino acids (shown in blue and purple) on the other. This arrangement is universal for a large number of AMPs, and such an amphipathic  $\alpha$ -helix structure is usually believed to be directly relevant to their antimicrobial function. The *de novo* modeled structure of Hc-CATH exhibits a helix-strand-helix conformation (Fig. 4C). The N-terminal region of Hc-CATH adopts a typical amphipathic  $\alpha$ -helix structure, in which the cationic amino acids (lysine and arginine residues, labeled in blue in shortened forms) concentrate on the upper side. Consistent with Fig. 4A, a short  $\alpha$ -helix presents in the C-terminal region of Hc-CATH and is linked to the N-terminal helix by a short-stranded region (Fig. 4C).

To confirm the accuracy of the predicted structures, CD spectroscopy was used to detect the secondary structures of Hc-CATH in solvents. Hc-CATH was dissolved in serial concentrations of SDS/H<sub>2</sub>O solution (0–120 mM) to an ultimate concentration of 0.2 mg/ml, and the CD spectra of the Hc-CATH solutions were recorded. As shown in Fig. 4D, the CD spectra of Hc-CATH dissolved in H<sub>2</sub>O showed a strong nega-

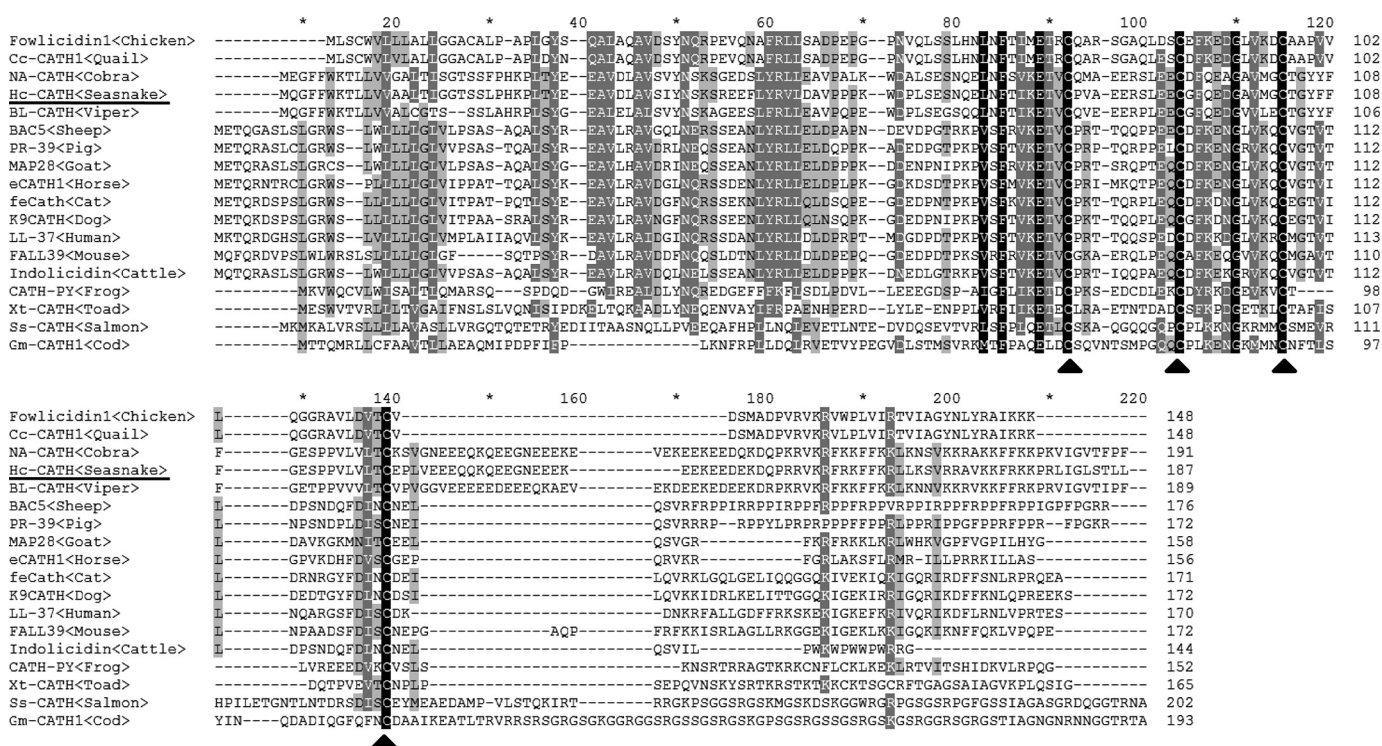


FIGURE 2. Multi-sequence alignment of Hc-CATH precursor with other representative cathelicidins. The identical residues are indicated in black. The highly conserved residues are shaded. The four conserved cysteines at the C terminus of the cathelin domain are marked with a triangle (▲).

tive peak at 200 nm, which indicates that Hc-CATH adopts a random-coil conformation. In contrast, in the membrane-mimetic environments of SDS/H<sub>2</sub>O solutions (30–120 nm), the CD spectra of Hc-CATH exhibited a strong positive peak at 190 nm and two negative peaks at 208 and 222 nm, which indicates that Hc-CATH mainly adopts an  $\alpha$ -helix conformation in hydrophobic or membrane-mimetic environments. Furthermore, the secondary structure components of Hc-CATH dissolved in 60 mM SDS/H<sub>2</sub>O were calculated as 59.9%  $\alpha$ -helix, 16%  $\beta$ -sheet, 0%  $\beta$ -turn, and 24% random coil. The secondary structures of Hc-CATH in high salt buffers and at high temperatures were also determined. As shown in Fig. 4F, the CD spectra of Hc-CATH treated at different temperatures were highly consistent, and the contents of different structure components did not show any obvious change. When dissolved in SDS/H<sub>2</sub>O solutions with serial concentrations of NaCl (at 0, 100, 200, and 400 mM), the  $\alpha$ -helix contents decreased slightly from 59.9 to 33.8% as the NaCl concentration increased. Simultaneously, the contents of the  $\beta$ -turn (0 to 14.9%) and random coil (24 to 30.5%) increased slightly. However, the mainly  $\alpha$ -helix secondary structure of Hc-CATH was maintained in high NaCl solutions (Fig. 4E).

**Antimicrobial Properties of Hc-CATH**—With ampicillin and meropenem used as positive controls, the antimicrobial potency of Hc-CATH toward human pathogens was first determined using a 2-fold broth microdilution method. As listed in Table 3, Hc-CATH displayed potent and broad-spectrum antimicrobial activity against 35 strains of the 48 human pathogenic microorganisms tested, with MICs ranging from 0.16 (toward *Shigella dysenteriae*) to 20.67 (toward *Klebsiella pneumoniae*) 8  $\mu$ M. Among the microorganisms tested, the clinical strain *S.*

*dysenteriae* exhibited the most sensitivity toward Hc-CATH, with an MIC value of 0.59  $\mu$ g/ml (0.16  $\mu$ M). Moreover, we observed that most of the tested microorganisms (28 strains of the 48) were ampicillin-resistant, but Hc-CATH could effectively kill them at low concentrations. Additionally, to understand the potential function of Hc-CATH in host anti-infective immune response, we collected 11 aquatic pathogenic bacteria, all of which are important pathogens that usually result in severe infectious diseases in marine animals. As indicated in Table 3, Hc-CATH showed potent antimicrobial activity against the 11 aquatic pathogens, with MICs ranging from 0.64 to 5.17  $\mu$ M. To investigate the effect of the  $\alpha$ -helix conformation and positive charge on the antimicrobial activity of Hc-CATH, we designed two Hc-CATH derivatives, Hc-CATH1 and -2 (with a decreasing positive charge but remaining in the  $\alpha$ -helix conformation), and an isotype control peptide, sHc-CATH (still having a positive charge identical to that of Hc-CATH but without the  $\alpha$ -helix conformation), and used a 2-fold broth microdilution method to determine their antimicrobial activities. As shown in Table 4, compared with Hc-CATH, Hc-CATH1 and Hc-CATH2 exhibited low antimicrobial activities against the tested bacteria, and the MIC values increased as the positive charge decreased (antimicrobial activity: Hc-CATH > Hc-CATH1 > Hc-CATH2). On the other hand, sHc-CATH did not show any antimicrobial activity against any of the tested bacteria.

To test the antimicrobial speed of Hc-CATH, a kinetic assay to measure bacterial killing was performed using a colony counting method. As illustrated in Table 5, Hc-CATH showed a rapid killing kinetic toward *E. coli* ATCC25922 within 60 min. More importantly, the cfu level remained at zero when the incubation time

## The First Cathelicidin from Sea Snakes

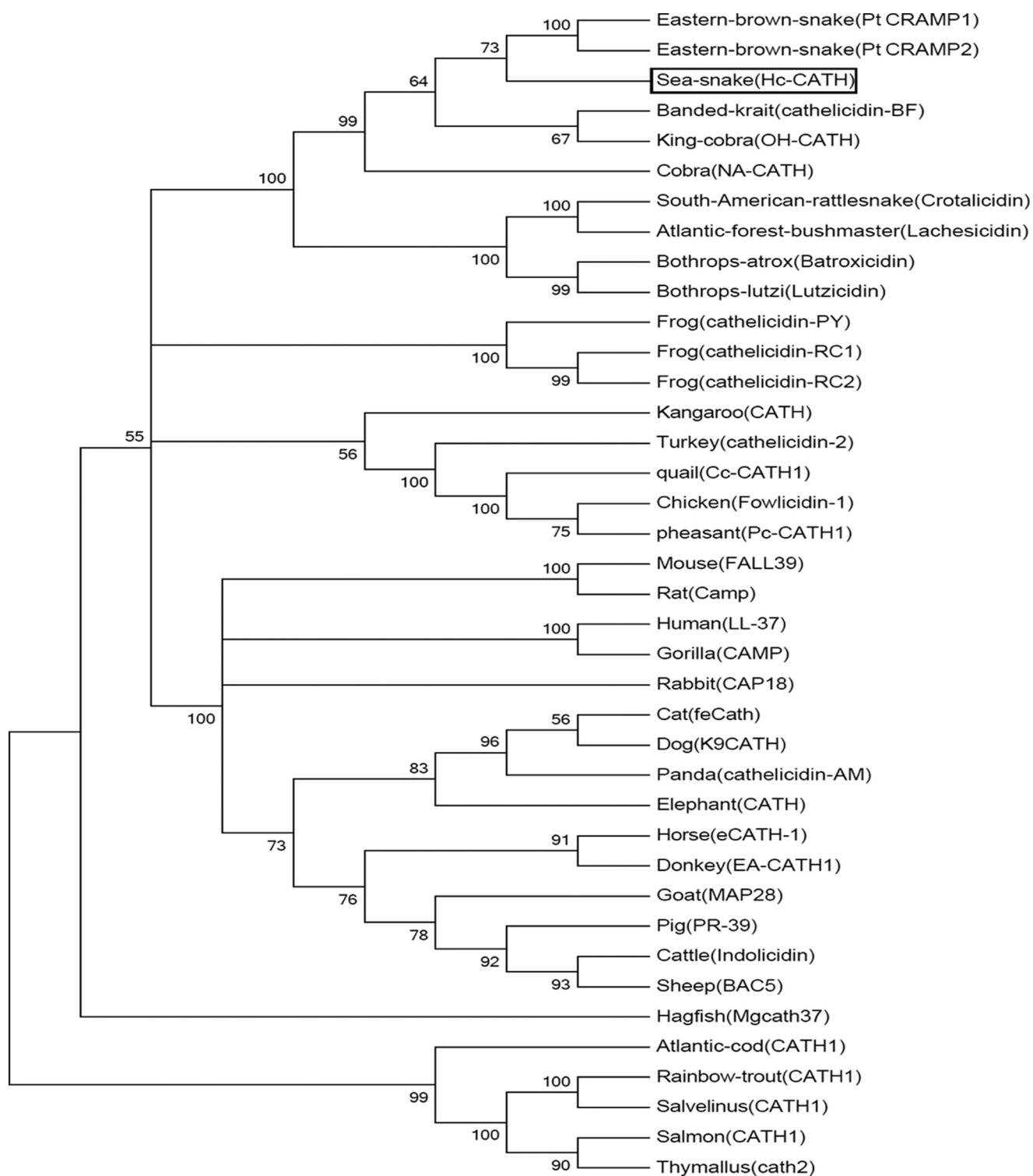


FIGURE 3. **Phylogenetic analysis of vertebrate cathelicidins.** The tree was constructed using the neighbor-joining method based on the proportional difference of the signal peptide and cathelin domain sequence of cathelicidins. A total of 1000 bootstrap replicates were used to test the reliability of each branch. Only bootstrap values > 50% are shown. Hc-CATH is boxed.

extended to 180 min, which implied that the antimicrobial effect of Hc-CATH was bactericidal rather than bacteriostatic. In contrast, it took 180 min for the positive control, meropenem, to completely eliminate *E. coli* ATCC25922 cells. Although the antimicrobial potency of Hc-CATH was less effective than meropenem (Table 3), the more rapid bactericidal action provides a remedy for its development as a novel antibiotic.

*Salt Tolerance, Thermal Tolerance, Thermal Stability, and Serum Stability of Hc-CATH*—It has been reported that the antimicrobial activity of many AMPs can be antagonized significantly by the presence of salt (29, 30). Therefore, in the present study, we studied the antimicrobial potency of Hc-CATH in salt solutions at different concentrations. As shown in Fig. 5A, the MIC value of Hc-CATH remained at 2.34  $\mu\text{g/ml}$  in a non-





# The First Cathelicidin from Sea Snakes

**TABLE 3**

**Antimicrobial activity of Hc-CATH**

CI, clinically isolated strain. The results represent the mean values of three independent experiments.

Microorganisms	MIC		
	Hc-CATH	Meropenem	Ampicillin
<i>μg/ml</i>			
<b>Gram-negative bacteria</b>			
<i>E. coli</i> ATCC25922	2.34 (0.64 $\mu\text{M}$ )	0.01 (0.03 $\mu\text{M}$ )	4.69 (12.62 $\mu\text{M}$ )
<i>E. coli</i> 1 (CI)	2.34 (0.64 $\mu\text{M}$ )	0.12 (0.31 $\mu\text{M}$ )	9.38 (25.24 $\mu\text{M}$ )
<i>E. coli</i> 2 (CI)	2.34 (0.64 $\mu\text{M}$ )	0.06 (0.15 $\mu\text{M}$ )	>200
<i>E. coli</i> 3 (CI)	2.34 (0.64 $\mu\text{M}$ )	0.03 (0.08 $\mu\text{M}$ )	>200
<i>E. coli</i> 4 (CI)	9.38 (2.59 $\mu\text{M}$ )	0.12 (0.31 $\mu\text{M}$ )	>200
<i>S. dysenteriae</i> (CI)	0.59 (0.16 $\mu\text{M}$ )	0.03 (0.08 $\mu\text{M}$ )	75.00 (201.90 $\mu\text{M}$ )
<i>K. pneumoniae</i> 1 (CI)	37.50 (10.33 $\mu\text{M}$ )	0.06 (0.15 $\mu\text{M}$ )	>200
<i>K. pneumoniae</i> 2 (CI)	4.69 (1.29 $\mu\text{M}$ )	0.06 (0.15 $\mu\text{M}$ )	>200
<i>K. pneumoniae</i> 3 (CI)	9.38 (2.59 $\mu\text{M}$ )	0.06 (0.15 $\mu\text{M}$ )	>200
<i>K. pneumoniae</i> 4 (CI)	9.38 (2.59 $\mu\text{M}$ )	0.06 (0.15 $\mu\text{M}$ )	>200
<i>K. pneumoniae</i> 5 (CI)	18.75 (5.17 $\mu\text{M}$ )	0.12 (0.31 $\mu\text{M}$ )	>200
<i>K. pneumoniae</i> 6 (CI)	37.50 (10.33 $\mu\text{M}$ )	0.12 (0.31 $\mu\text{M}$ )	>200
<i>K. pneumoniae</i> 7 (CI)	37.50 (10.33 $\mu\text{M}$ )	0.12 (0.31 $\mu\text{M}$ )	>200
<i>K. pneumoniae</i> 8 (CI)	75.00 (20.67 $\mu\text{M}$ )	0.12 (0.31 $\mu\text{M}$ )	>200
<i>Serratia marcescens</i> (CI)	>200	0.06 (0.15 $\mu\text{M}$ )	37.50 (100.90 $\mu\text{M}$ )
<i>Klebsiella oxytoca</i> (CI)	4.69 (1.29 $\mu\text{M}$ )	0.12 (0.31 $\mu\text{M}$ )	>200
<i>Proteus vulgaris</i> (CI)	>200	0.23 (0.61 $\mu\text{M}$ )	18.75 (50.49 $\mu\text{M}$ )
<i>Proteus mirabilis</i> (CI)	4.69 (1.29 $\mu\text{M}$ )	0.47 (1.22 $\mu\text{M}$ )	75.00 (201.90 $\mu\text{M}$ )
<i>Acinetobacter baumannii</i> 1 (CI)	>200	0.23 (0.61 $\mu\text{M}$ )	37.50 (100.90 $\mu\text{M}$ )
<i>A. baumannii</i> 2 (CI)	>200	0.23 (0.61 $\mu\text{M}$ )	9.38 (25.24 $\mu\text{M}$ )
<i>Stenotrophomonas maltophilia</i> 1 (CI)	>200	4.69 (12.22 $\mu\text{M}$ )	18.75 (50.49 $\mu\text{M}$ )
<i>S. maltophilia</i> 2 (CI)	9.38 (2.59 $\mu\text{M}$ )	4.69 (12.22 $\mu\text{M}$ )	>200
<i>Pseudomonas aeruginosa</i> ATCC27853	18.75 (5.17 $\mu\text{M}$ )	0.06 (0.15 $\mu\text{M}$ )	>200
<i>P. aeruginosa</i> 1 (CI)	37.50 (10.33 $\mu\text{M}$ )	0.06 (0.15 $\mu\text{M}$ )	9.38 (25.24 $\mu\text{M}$ )
<i>P. aeruginosa</i> 2 (CI)	>200	1.88 (4.89 $\mu\text{M}$ )	>200
<i>Salmonella paratyphi A</i> (CI)	4.69 (1.29 $\mu\text{M}$ )	0.12 (0.31 $\mu\text{M}$ )	>200
<b>Gram-positive bacteria</b>			
<i>S. aureus</i> ATCC25923	4.69 (1.29 $\mu\text{M}$ )	0.06 (0.15 $\mu\text{M}$ )	9.38 (25.24 $\mu\text{M}$ )
<i>S. aureus</i> 1 (CI)	>200	0.06 (0.15 $\mu\text{M}$ )	18.75 (50.49 $\mu\text{M}$ )
<i>S. aureus</i> 2 (CI)	>200	0.12 (0.31 $\mu\text{M}$ )	>200
<i>S. aureus</i> 3 (CI)	>200	18.75 (48.9 $\mu\text{M}$ )	>200
<i>S. aureus</i> 4 (CI)	4.69 (1.29 $\mu\text{M}$ )	0.12 (0.31 $\mu\text{M}$ )	9.38 (25.24 $\mu\text{M}$ )
<i>S. aureus</i> 5 (CI)	4.69 (1.29 $\mu\text{M}$ )	0.06 (0.15 $\mu\text{M}$ )	9.38 (25.24 $\mu\text{M}$ )
<i>Bacillus cereus</i> (CI)	9.38 (2.59 $\mu\text{M}$ )	0.06 (0.15 $\mu\text{M}$ )	>200
<i>Bacillus subtilis</i> (CI)	75.00 (20.67 $\mu\text{M}$ )	0.03 (0.08 $\mu\text{M}$ )	75.00 (201.90 $\mu\text{M}$ )
<i>Enterococcus faecium</i> (CI)	37.50 (10.33 $\mu\text{M}$ )	9.38 (24.45 $\mu\text{M}$ )	>200
<i>Nocardia asteroides</i> (CI)	9.38 (2.59 $\mu\text{M}$ )	4.69 (12.22 $\mu\text{M}$ )	18.75 (50.49 $\mu\text{M}$ )
<i>Enterococcus faecalis</i> (CI)	>200	9.38 (24.45 $\mu\text{M}$ )	37.50 (100.90 $\mu\text{M}$ )
<i>Staphylococcus epidermidis</i> (CI)	>200	0.94 (2.45 $\mu\text{M}$ )	>200
<b>Fungi</b>			
<i>Candida albicans</i> 1 (CI)	4.69 (1.29 $\mu\text{M}$ )	0.12 (0.31 $\mu\text{M}$ )	>200
<i>C. albicans</i> 2 (CI)	4.69 (1.29 $\mu\text{M}$ )	0.23 (0.61 $\mu\text{M}$ )	>200
<i>C. albicans</i> 3 (CI)	4.69 (1.29 $\mu\text{M}$ )	0.06 (0.15 $\mu\text{M}$ )	>200
<i>C. albicans</i> 4 (CI)	4.69 (1.29 $\mu\text{M}$ )	0.12 (0.31 $\mu\text{M}$ )	18.75 (50.49 $\mu\text{M}$ )
<i>C. albicans</i> 5 (CI)	2.34 (0.64 $\mu\text{M}$ )	0.06 (0.15 $\mu\text{M}$ )	>200
<i>C. albicans</i> 6 (CI)	2.34 (0.64 $\mu\text{M}$ )	0.03 (0.08 $\mu\text{M}$ )	>200
<i>Candida glabrata</i> 1 (CI)	2.34 (0.64 $\mu\text{M}$ )	0.03 (0.08 $\mu\text{M}$ )	18.75 (50.49 $\mu\text{M}$ )
<i>C. glabrata</i> 2 (CI)	>200	0.06 (0.15 $\mu\text{M}$ )	>200
<i>Cryptococcus neoformans</i> (CI)	>200	0.47 (1.22 $\mu\text{M}$ )	4.69 (12.62 $\mu\text{M}$ )
<i>Arcyria cinerea</i>	9.38 (2.59 $\mu\text{M}$ )	0.12 (0.31 $\mu\text{M}$ )	>200
<b>Aquatic pathogenic bacteria</b>			
<i>Aeromonas sobria</i>	2.34 (0.64 $\mu\text{M}$ )	0.03 (0.08 $\mu\text{M}$ )	>200
<i>Aeromonas hydrophila</i>	2.34 (0.64 $\mu\text{M}$ )	0.06 (0.15 $\mu\text{M}$ )	>200
<i>Aeromonas veronii</i>	2.34 (0.64 $\mu\text{M}$ )	0.03 (0.08 $\mu\text{M}$ )	>200
<i>Vibrio vulnificus</i>	4.69 (1.29 $\mu\text{M}$ )	0.12 (0.31 $\mu\text{M}$ )	75.00 (201.90 $\mu\text{M}$ )
<i>Vibrio harveyi</i>	9.38 (2.59 $\mu\text{M}$ )	0.03 (0.08 $\mu\text{M}$ )	37.50 (100.90 $\mu\text{M}$ )
<i>Vibrio fluvialis</i>	4.69 (1.29 $\mu\text{M}$ )	0.23 (0.61 $\mu\text{M}$ )	75.00 (201.90 $\mu\text{M}$ )
<i>Vibrio alginolyticus</i>	4.69 (1.29 $\mu\text{M}$ )	0.12 (0.31 $\mu\text{M}$ )	>200
<i>Vibrio parahaemolyticus</i>	9.38 (2.59 $\mu\text{M}$ )	0.47 (1.22 $\mu\text{M}$ )	18.75 (50.49 $\mu\text{M}$ )
<i>Vibrio splendidus</i>	2.34 (0.64 $\mu\text{M}$ )	0.47 (1.22 $\mu\text{M}$ )	>200
<i>Vibrio anguillarum</i>	18.75 (5.17 $\mu\text{M}$ )	0.23 (0.61 $\mu\text{M}$ )	>200
<i>Edwardsiella tarda</i>	2.34 (0.64 $\mu\text{M}$ )	0.12 (0.31 $\mu\text{M}$ )	>200

an essential characteristic of AMPs that needs to be carefully investigated. As shown in Fig. 5B, after incubation in different temperatures for 1 h, Hc-CATH maintained its potent antimicrobial activity with the MIC value remaining in the range of 1.95 to 4.69  $\mu\text{g/ml}$ .

Many traditional antibiotics, including  $\beta$ -lactam antibiotics, cephalosporins, tetracyclines, and quinolones, are often unsta-

ble in aqueous solutions, which significantly restricts their usage (31, 32). In contrast, Hc-CATH is extremely stable in aqueous solution (Fig. 5C). After incubated at 37  $^{\circ}\text{C}$  for 96 h, the MIC value of Hc-CATH solution against *E. coli* ATCC25922 increased only  $\sim$ 2-fold from 1.56 to 3.91  $\mu\text{g/ml}$ .

It has been reported that many AMPs have low stability *in vivo* and are susceptible to degradation by both endogenous

human proteases and proteases secreted by pathogens (33). Peptide degradation by serum proteases and their interaction with serum components generally influence the antimicrobial activity of AMPs. As a result, in the present study we examined the effect of human serum on the antimicrobial activity of Hc-CATH. As shown in Fig. 5D, the MIC values of Hc-CATH against *E. coli* ATCC25922 gradually increased from 2.34 to 37.5  $\mu\text{g/ml}$  with extended incubation, which indicates that sim-

ilar to many other AMPs, Hc-CATH can be degraded and bound by human serum proteins. However, Hc-CATH retained its potent antimicrobial activity even after incubation with human serum for 6 h, showing it to be far more stable than the previously described cathelicidins from terrestrial snakes (22, 34).

**Cytotoxicity and Hemolysis of Hc-CATH**—As shown in Table 6, Hc-CATH exhibited very low cytotoxicity toward the tested mammalian cells. At concentrations up to 200  $\mu\text{g/ml}$  (55.12  $\mu\text{M}$ , nearly 10-fold high than the MICs of most tested microorganisms), Hc-CATH induced cell death percentages as low as 4.70, 3.63, 1.30, and 4.28% for HepG2, PC3, L929, and mouse peritoneal macrophage cells, respectively. As to hemolytic activity, Hc-CATH yielded a hemolysis of 5.25%, at the same concentration of 200  $\mu\text{g/ml}$ .

**Hc-CATH Binds to Bacteria and Induces Alteration of Microbial Membrane Morphology**—Attraction and attachment to microbial surfaces is regarded as the first step for AMP-mediated cell killing (10). Therefore, we used flow cytometry to

**TABLE 4**  
Antimicrobial activity comparison of Hc-CATH and its derivatives

Microorganisms	MIC			
	Hc-CATH	Hc-CATH1	Hc-CATH2	sHc-CATH
<i>E. coli</i> ATCC25922	2.34	18.75	>200	>200
<i>P. aeruginosa</i> ATCC27853	18.75	18.75	37.5	>200
<i>Staphylococcus aureus</i> ATCC25923	4.69	>200	>200	>200
<i>C. albicans</i> 1 (CI) <sup>a</sup>	4.69	18.75	75	>200
<i>A. hydrophila</i>	2.34	4.69	9.38	>200
<i>V. parahaemolyticus</i>	9.38	18.75	75	>200

<sup>a</sup> CI, clinically isolated strain.

**TABLE 5**  
Killing kinetics of Hc-CATH against *E. coli* ATCC25922

*E. coli* ATCC25922 was mixed with Hc-CATH at a concentration of  $5 \times \text{MIC}$  for 0, 10, 20, 30, 45, 60, 90, 120, and 180 min. The MICs of Hc-CATH and meropenem against *E. coli* ATCC25922 are 2.34 and 0.01  $\mu\text{g/ml}$ , respectively. The results represent mean values of three independent experiments.

Peptide	Time									
	0 min	10 min	20 min	30 min	45 min	60 min	90 min	120 min	180 min	
Hc-CATH	75 $\pm$ 11.0	39 $\pm$ 5.0	42 $\pm$ 28.5	21 $\pm$ 5.3	6 $\pm$ 5.0	0 $\pm$ 0.0	0 $\pm$ 0.0	0 $\pm$ 0.0	0 $\pm$ 0.0	
Meropenem	78 $\pm$ 8.7	98 $\pm$ 11.7	82 $\pm$ 12.1	90 $\pm$ 14.9	63 $\pm$ 40.7	69 $\pm$ 15.5	1 $\pm$ 1.7	0.3 $\pm$ 0.6	0 $\pm$ 0.0	
Control	93 $\pm$ 8.1	81 $\pm$ 20.8	96 $\pm$ 10.1	104 $\pm$ 30.5	96 $\pm$ 42.6	168 $\pm$ 17.9	387 $\pm$ 20.1	637 $\pm$ 115.8	1104 $\pm$ 145.7	

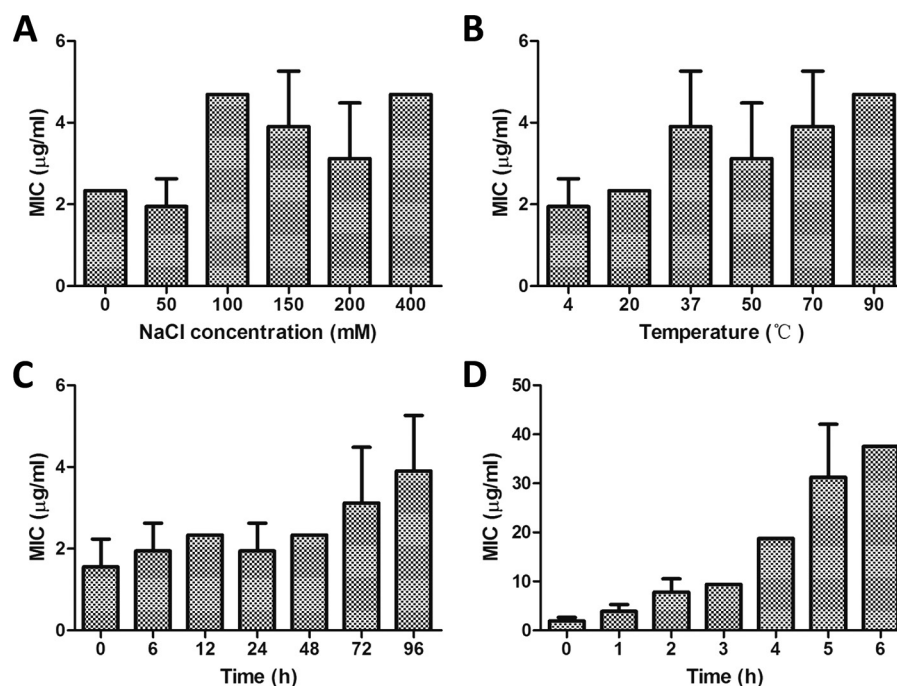


**FIGURE 5. Stability of Hc-CATH.** A, salt tolerance of Hc-CATH. MICs of Hc-CATH against *E. coli* ATCC25922 are shown in the presence of 0, 50, 100, 150, 200, and 400 mM sodium chloride. B, thermal tolerance of Hc-CATH. Hc-CATH solution (2 mg/ml, dissolved in sterile deionized water) was incubated at different temperatures (4, 20, 37, 50, 70, and 90 °C) for 1 h, and then the MICs against *E. coli* ATCC25922 were determined. C, thermal stability of Hc-CATH solution at 37 °C. Hc-CATH solution was incubated at 37 °C for 0 to 96 h, and then the MICs against *E. coli* ATCC25922 were determined. D, effect of human serum on the antimicrobial activity of Hc-CATH. Hc-CATH was incubated with human serum (1:4 (v/v)) at 37 °C for 0 to 6 h, and MICs of the samples against *E. coli* ATCC25922 were determined at each time point. The results represent the mean values of three independent experiments.

## The First Cathelicidin from Sea Snakes

investigate the interaction of Hc-CATH with bacterial cells. As illustrated in Fig. 6, *A* and *B*, a 5-min incubation allowed Hc-CATH to rapidly bind to *E. coli* ATCC25922 and *S. aureus* ATCC25923 cells. It has been reported that many cathelicidins

kill microbial cells through permeabilization of the cytoplasmic membrane (24, 35). Permeabilization of the cytoplasmic membrane causes a disruption of microbial cell integrity, which results in an obvious cell morphological alteration and can be clearly observed by SEM. As illustrated in Fig. 6, *C–F*, the control *S. aureus* ATCC25923 and *E. coli* ATCC25922 cells exhibited a normal shape and smooth surface (Fig. 6, *C* and *E*). After the treatment with Hc-CATH ( $5 \times \text{MIC}$ ) for 30 min, obvious cell swelling and deformation emerged, especially for *E. coli* ATCC25922 cells (Fig. 6, *D* and *F*). The cells were disrupted, and a large amount of cellular inclusions leaked out to the cell surface (Fig. 6, *D* and *F*, indicated by *arrows*), which implies that Hc-CATH can induce microbial membrane permeabilization resulting in cellular disruption of both Gram-positive and Gram-negative bacteria.

**TABLE 6**  
Cytotoxicity and Hemolysis of Hc-CATH

The ultimate concentration of Hc-CATH in the assay was 200  $\mu\text{g/ml}$ . The results represent mean values of three independent experiments.

Cells	Cell death/Hemolysis %
HepG2	4.70
PC3	3.63
L929	1.30
Mouse peritoneal macrophages	4.28
Human erythrocytes	5.25

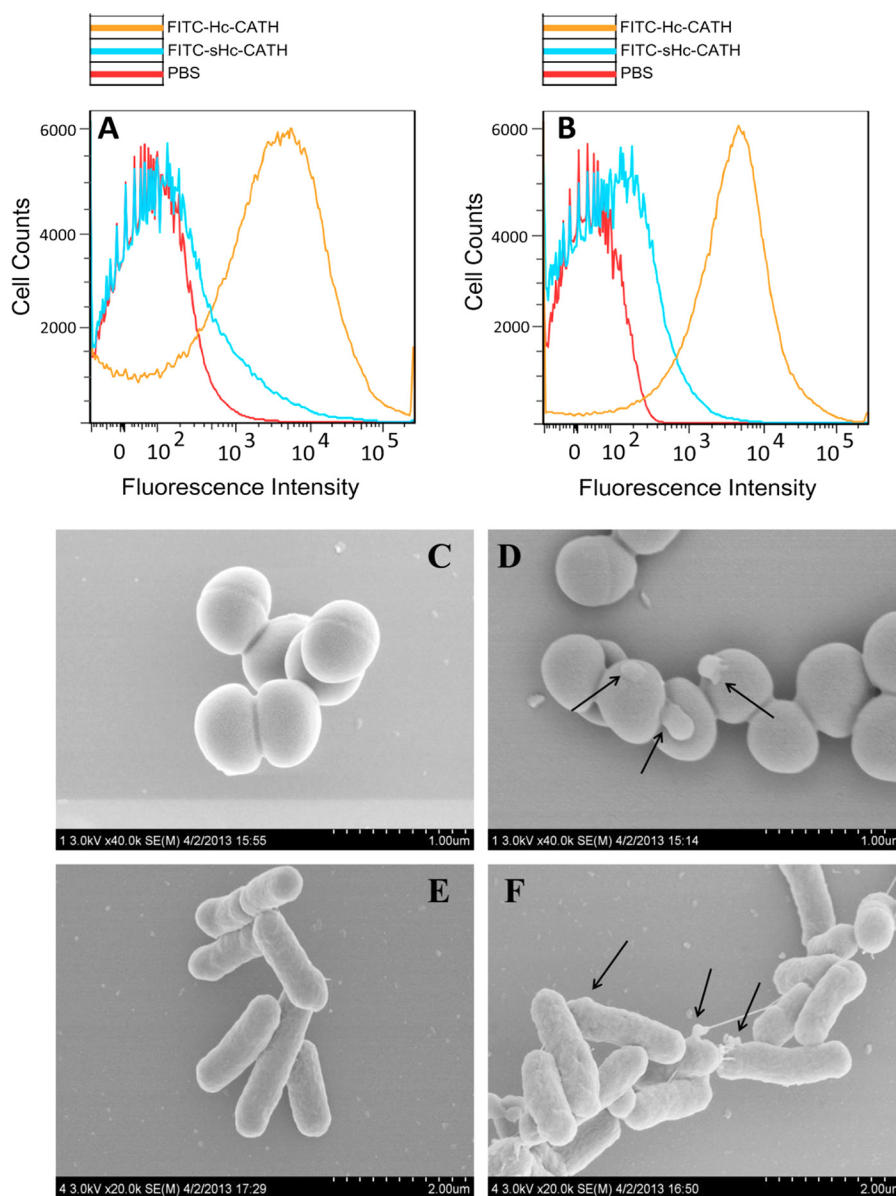


**FIGURE 6. Antimicrobial mechanism of Hc-CATH.** Hc-CATH rapidly bind to *E. coli* ATCC25922 (*A*) and *S. aureus* ATCC25923 (*B*). Hc-CATH results in the disruption and morphological alteration of bacterial cells: control *S. aureus* ATCC25923 (*C*); Hc-CATH-treated *S. aureus* ATCC25923 (*D*); control *E. coli* ATCC25922 (*E*); Hc-CATH-treated *E. coli* ATCC25922 (*F*). The *arrows* in *D* and *F* indicate damage to the microbial membranes or the cellular inclusion efflux induced by Hc-CATH.

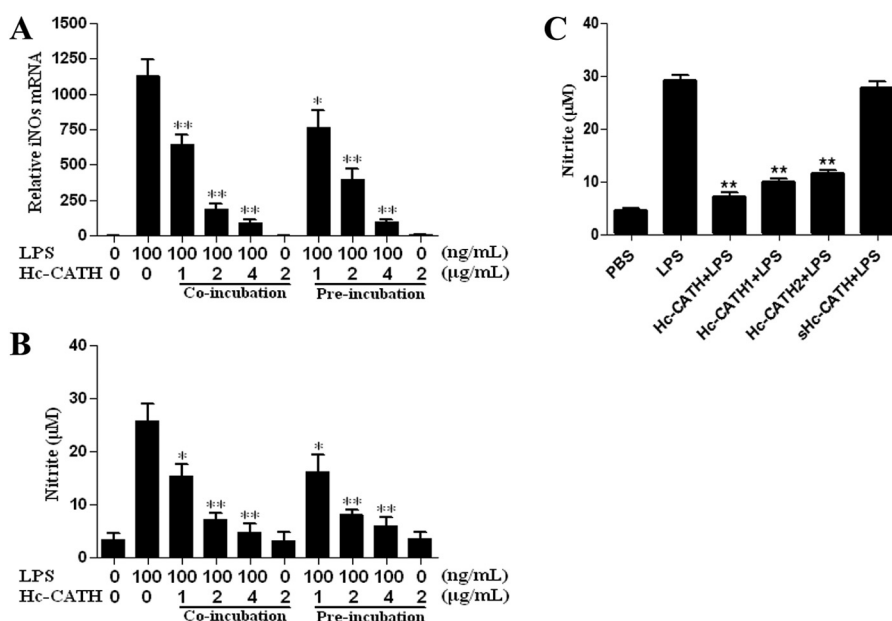


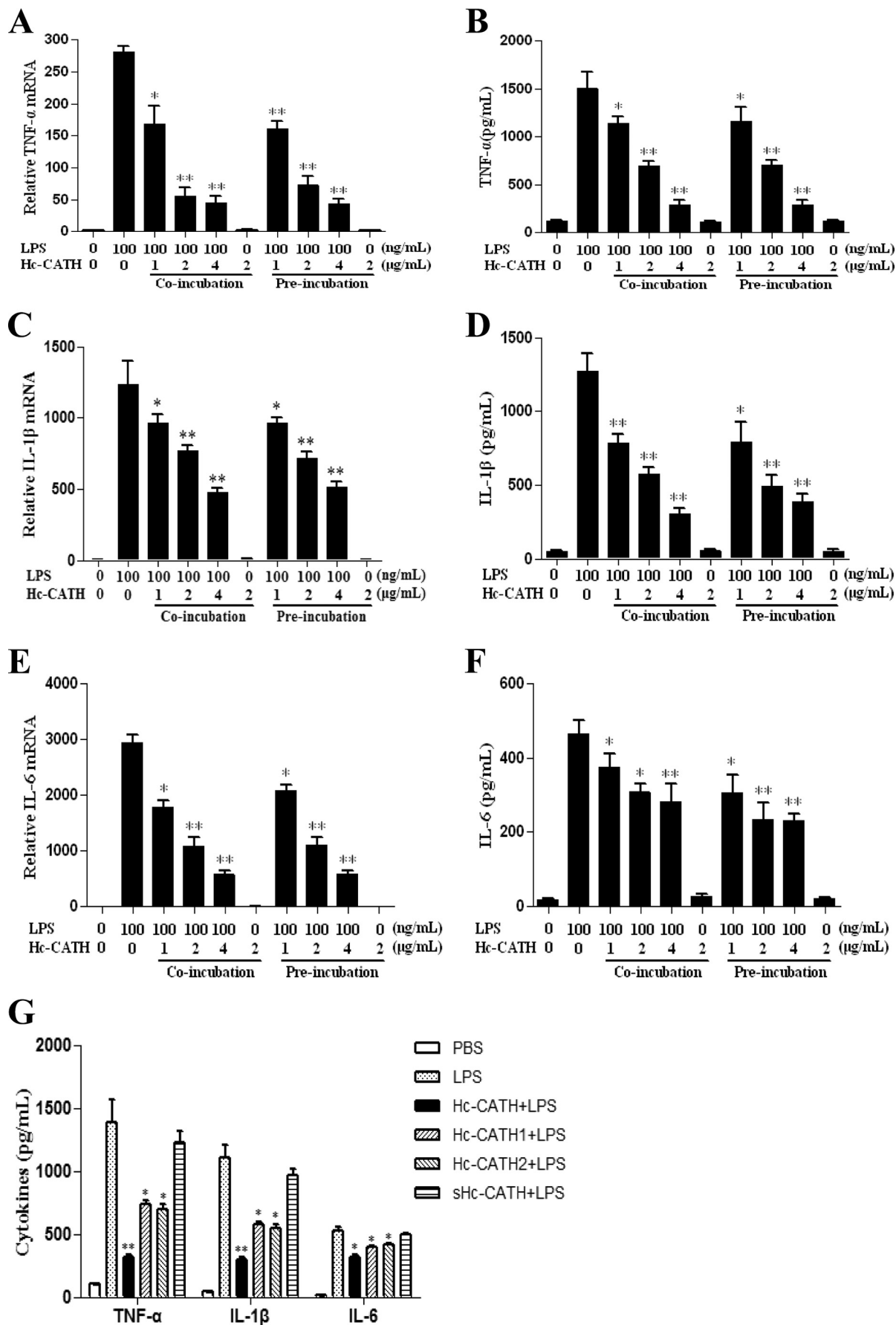
FIGURE 7. **Effects of Hc-CATH on iNOS transcription and NO production induced by LPS.** A, iNOS transcription. B, nitrite production. C, effects of sHc-CATH, Hc-CATH1, and Hc-CATH2 on LPS-induced NO production. LPS, 100 ng/ml; peptides, 4 µg/ml. Data are mean  $\pm$  S.E. values from three separate experiments. \*,  $p < 0.05$ ; \*\*,  $p < 0.01$  (significantly different compared with the control).

**Hc-CATH Reduces LPS-induced iNOS Transcription and NO Production**—To determine the effect of Hc-CATH on the LPS-induced NO production in MPMs, we first used qRT-PCR to determine the mRNA level of iNOS, the enzyme required to generate NO. As shown in Fig. 7A, 100 ng/ml LPS greatly increased the iNOS transcription to  $\sim$ 600-fold compared with that of untreated cells. Co-incubation with Hc-CATH or preincubation with Hc-CATH for 30 min significantly reduced the mRNA level of iNOS induced by LPS in a dose-dependent manner. At a concentration of 4 µg/ml, Hc-CATH inhibited  $>90\%$  of the iNOS transcription for both the co-incubation and the preincubation groups. Furthermore, we determined the NO production by examining the nitrite concentration in the MPM culture supernatants. As illustrated in Fig. 7B, 100 ng/ml LPS induced 25.7 µM nitrite production. When co-incubated with Hc-CATH and/or preincubated with Hc-CATH for 30 min, the nitrite concentrations were reduced significantly. At the concentration of 4 µg/ml, Hc-CATH inhibited 81% of nitrite production for the co-incubation group and 76.9% for the preincubation group, which indicates the strong inhibitory effect of Hc-CATH on NO production in MPMs induced by LPS. The inhibitory effects of sHc-CATH and Hc-CATH1 and -2 on LPS-induced NO productions were also determined. As shown in Fig. 7C, similar to Hc-CATH, at a concentration of 4 µg/ml, the derivatives Hc-CATH1 and -2 significantly inhibited the LPS-induced NO production in MPM cells. However, the inhibitory effects of Hc-CATH1 and -2 were less potent than Hc-CATH, and Hc-CATH2 exhibited the weakest activity. Besides, unlike Hc-CATH1 and -2, sHc-CATH did not show a significant inhibitory effect, which implies the importance of the amphipathic  $\alpha$ -helical structure on the anti-inflammatory activities of the peptides.

**Hc-CATH Inhibits LPS-induced Pro-inflammatory Cytokine Production**—To evaluate the effect of Hc-CATH on LPS-induced pro-inflammatory cytokine production in MPMs, we

first used qRT-PCR to determine pro-inflammatory cytokine gene expression. Hc-CATH (2 µg/ml), whether co-incubated or preincubated with MPM cells in the absence of LPS, did not alter the gene expression of TNF- $\alpha$ , IL-1 $\beta$ , and IL-6 (Fig. 8A, C, and E). However, Hc-CATH significantly blocked LPS-induced expression of TNF- $\alpha$ , IL-1 $\beta$ , and IL-6 in a dose-dependent manner. In fact, Hc-CATH inhibited the expression of all three of the pro-inflammatory cytokine genes by  $>60\%$  at 4 µg/ml, especially for TNF- $\alpha$  and IL-6 ( $>80\%$ ), in both the co-incubation and the preincubation groups (Fig. 8, A, C, and E). Furthermore, we used ELISA to confirm the effect of Hc-CATH on pro-inflammatory cytokine production induced by LPS in MPMs. 100 ng/ml LPS alone induced the production of TNF- $\alpha$ , IL-1 $\beta$ , and IL-6 for about 1500, 1270, and 464 pg/ml, respectively. Consistent with the result of qRT-PCR, Hc-CATH significantly inhibited the production of TNF- $\alpha$ , IL-1 $\beta$  and IL-6 in a dose-dependent manner (Fig. 8, B, D, and F). For the co-incubation group, 4 µg/ml Hc-CATH inhibited LPS-induced TNF- $\alpha$ , IL-1 $\beta$ , and IL-6 production by 81, 76, and 40%, respectively. For the preincubation group, at the same concentration of Hc-CATH (4 µg/ml), the cytokine levels (287, 387, and 231 pg/ml for TNF- $\alpha$ , IL-1 $\beta$ , and IL-6, respectively) were comparable with those of the co-incubation group (292, 305, and 283 pg/ml for TNF- $\alpha$ , IL-1 $\beta$ , and IL-6, respectively). As shown in Fig. 8G, the derivatives Hc-CATH1 and -2 also exhibited significant inhibitory effects on LPS-induced TNF- $\alpha$ , IL-1 $\beta$ , and IL-6 production, but their activities were less potent than Hc-CATH, which implies that the positive charge of Hc-CATH was an important factor for anti-inflammatory activity. Moreover, consistent with NO production, sHc-CATH did not exhibit an apparent inhibitory effect on the production of TNF- $\alpha$ , IL-1 $\beta$ , and IL-6.

**Hc-CATH Inhibits LPS-induced Inflammatory Response Pathways**—The above data indicate that Hc-CATH significantly inhibited the transcription and production of TNF- $\alpha$ ,



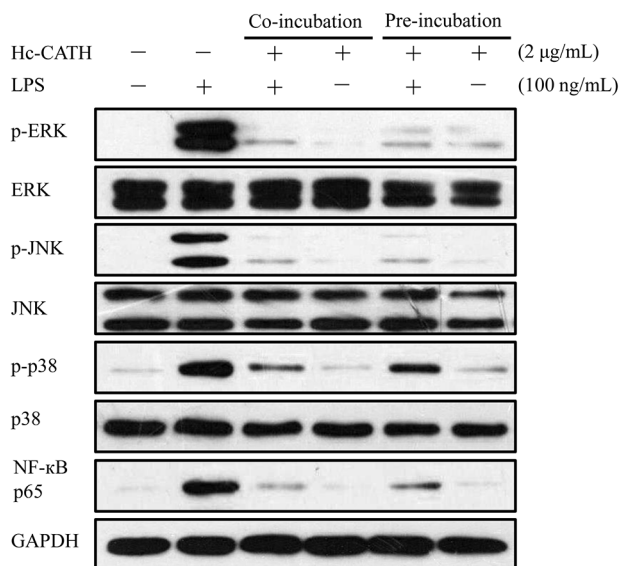


**FIGURE 9. Effects of Hc-CATH on LPS-induced inflammatory response pathways.** Western blot of phosphorylation of ERK, JNK, and p38 and the translocation of the NF- $\kappa$ B p65 subunit from cytoplasm to nucleus in MPM cells. MPM cells were co-incubated with LPS (100 ng/ml) and Hc-CATH (2  $\mu$ g/ml) or preincubated with Hc-CATH (2  $\mu$ g/ml) for 15 min before the addition of LPS (100 ng/ml). After incubation for 30 min, the cells were collected, and the cytoplasmic or nuclear proteins were extracted for Western blot analysis.

IL-1 $\beta$ , IL-6, and NO, which were induced by LPS in MPM cells. LPS, also known as an endotoxin, is an effective agonist of TLR4. Binding of LPS to TLR4 on the cell membrane leads to the activation of inflammatory signaling pathways. Several mitogen-activated protein kinases (MAPKs), such as extracellular signal-regulated kinase (ERK), p38, and c-Jun N-terminal kinase (JNK), are sequentially phosphorylated (activated), and ultimately the transcription factor NF- $\kappa$ B translocates into the nucleus, which stimulates the expression of pro-inflammatory cytokines (4). Therefore, we studied the effect of Hc-CATH on LPS-induced inflammatory signaling pathways. As shown in Fig. 9, 100 ng/ml LPS significantly induced the phosphorylation of ERK, JNK, p38, and the translocation of the NF- $\kappa$ B p65 subunit from cytoplasm to nucleus. Furthermore Hc-CATH (2  $\mu$ g/ml) alone did not exhibit any effects similar to LPS. In contrast, the co-incubation or preincubation of Hc-CATH (2  $\mu$ g/ml) markedly inhibited the LPS-induced phosphorylation of ERK, JNK, and p38 and translocation of the NF- $\kappa$ B p65 subunit, which indicates that Hc-CATH executes its anti-inflammatory effect through inhibition of MAPKs and NF- $\kappa$ B inflammatory signaling pathways.

**Hc-CATH Binds and Neutralizes LPS**—To evaluate whether the inhibition of LPS-induced proinflammatory responses occurs partly through the direct binding of Hc-CATH to LPS, the new MST technique was used. A titration series of Hc-CATH was performed over a range of 67.14 nM to 137.5  $\mu$ M while FITC-LPS was kept constant at 3.375  $\mu$ M throughout the series. Upon binding of Hc-CATH to FITC-LPS, the thermo-

phoretic signal changed, as shown in Fig. 10A. The binding data were further fitted with the Hill method, and a dissociation constant,  $K_d$  of  $25.2 \pm 0.68$   $\mu$ M, was yielded, which provided evidence for the direct binding of Hc-CATH to LPS. Furthermore, we used a sensitive chromogenic LAL assay to determine whether the binding of Hc-CATH to LPS can neutralize its toxicity. As shown in Fig. 10B, Hc-CATH exhibited an obvious concentration-dependent LPS neutralizing activity. At the concentration of 64  $\mu$ M, Hc-CATH inhibited >50% of LPS. In contrast, sHc-CATH did not show significant LPS neutralizing activity.

**Hc-CATH Binds to MPM Cells and Blocks TLR4**—To investigate whether Hc-CATH has a binding effect on MPM cells, flow cytometry experiments were carried out. As illustrated in Fig. 11A, Hc-CATH bound directly to MPM cells after a 15-min preincubation. To evaluate the interaction of Hc-CATH and TLR4 in MPM cells, we next used a monoclonal TLR4 antibody (PE-anti-TLR4) to stain the MPM cells. As illustrated in Fig. 11B, the existence of Hc-CATH (2  $\mu$ g/ml) significantly decreased the fluorescence intensity (23%) of MPM cells, which indicates that Hc-CATH could block TLR4 to inhibit its binding with PE-anti-TLR4 (Fig. 11B).

**Hc-CATH Binds to TLR4/MD2 and Overlaps the LPS-binding Pocket**—TLR4 alone lacks the ability to sense LPS, thus the need to associate with MD2 to form the TLR4/MD2 heterodimer receptor complex (36). MD2 is the component of the TLR4/MD2 complex that interacts directly with LPS (37). LPS binding induces dimerization of the TLR4/MD2 complex, and aggregation of the complex leads to activation of subsequent multiple signaling pathways (36). According to the results of molecular docking, Hc-CATH bound to the TLR4/MD2 complex, and the binding site was significantly closer to MD2 (Fig. 12, B and C). The elaborate docking structure of Hc-CATH and MD2 indicates that Hc-CATH is located at the entrance of the LPS-binding pocket in MD2 (Fig. 12D), which implies that Hc-CATH binds to the TLR4/MD2 complex and overlaps the LPS-binding pocket in MD2, thereby blocking the binding of LPS to MD2 and the subsequent activation of signaling pathways.

## Discussion

Snakes, among the oldest known vertebrates, are highly different in morphology and thrive in diverse ecological environments. They possess an ancient but powerful innate immune system, which has enabled them to survive successfully over millions of years of evolution (38). Gene-encoded antimicrobial peptides represent the main component of an innate immune system that protects snakes from microbial infections. However, compared with amphibians, from which more than 600 AMPs belonging to more than 30 families have been identified, less than 30 AMPs have been identified from the diverse species of snake. Most of the snake AMPs that have been identified belong to the cathelicidin and defensin families. Moreover, only

**FIGURE 8. Effects of Hc-CATH on pro-inflammatory cytokines transcription and production induced by LPS.** A, TNF- $\alpha$  mRNA. B, TNF- $\alpha$  production. C, IL-1 $\beta$  mRNA. D, IL-1 $\beta$  production. E, IL-6 mRNA. F, IL-6 production. G, effects of sHc-CATH, Hc-CATH1 and -2 on LPS-induced pro-inflammatory cytokines production. LPS, 100 ng/ml; peptides, 4  $\mu$ g/ml. Data are mean  $\pm$  S.E. values from three separate experiments. \*,  $p < 0.05$ ; \*\*,  $p < 0.01$  (significantly different compared with the control).

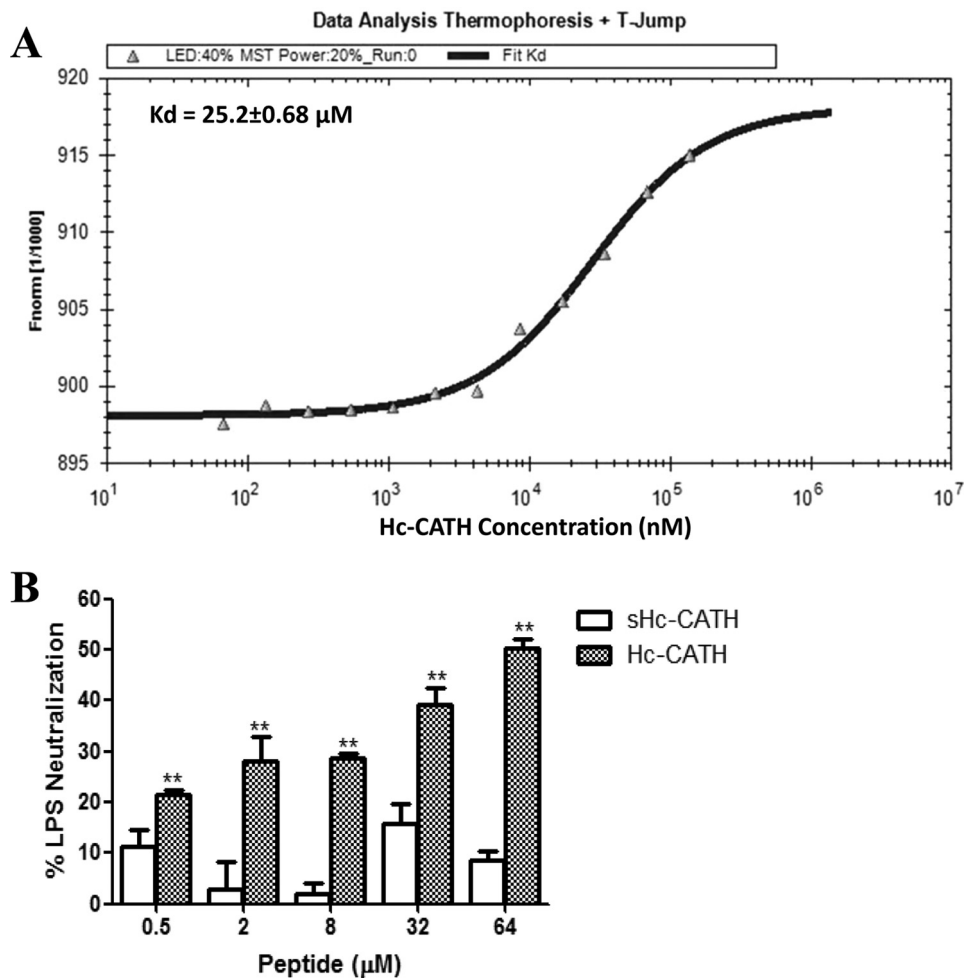


FIGURE 10. **Binding and neutralization of LPS by Hc-CATH.** *A*, Hc-CATH binds to LPS by MST measurement. The x axis represents Hc-CATH concentrations, and the y axis represents the normalized fluorescence. The curve represents a fit of the binding data giving a  $K_d$  of  $25.2 \pm 0.68 \mu\text{M}$ . *B*, LPS neutralization by Hc-CATH. A sensitive chromogenic LAL assay was used to evaluate the neutralization of LPS by Hc-CATH. Data shown are mean  $\pm$  S.E. values from three independent experiments (\*\*,  $p < 0.01$ ).

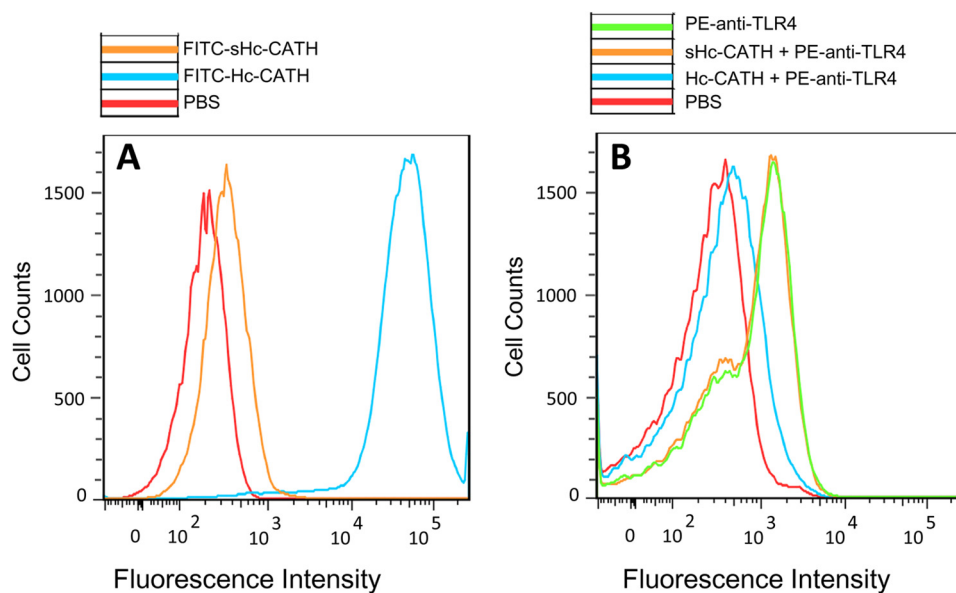


FIGURE 11. **Hc-CATH binds to MPMs and blocks TLR4.** *A*, MPM cells were incubated with FITC-Hc-CATH or FITC-sHc-CATH ( $2 \mu\text{g/ml}$ ) for 15 min at  $37^\circ\text{C}$  before assay. *B*, Hc-CATH binds to TLR4 on the surface of MPMs. MPM cells were preincubated with Hc-CATH or sHc-CATH ( $2 \mu\text{g/ml}$ ) at  $37^\circ\text{C}$  for 15 min and then were stained with anti-mouse PE-TLR4 ( $2 \mu\text{g/ml}$ ) for 30 min at  $4^\circ\text{C}$ .



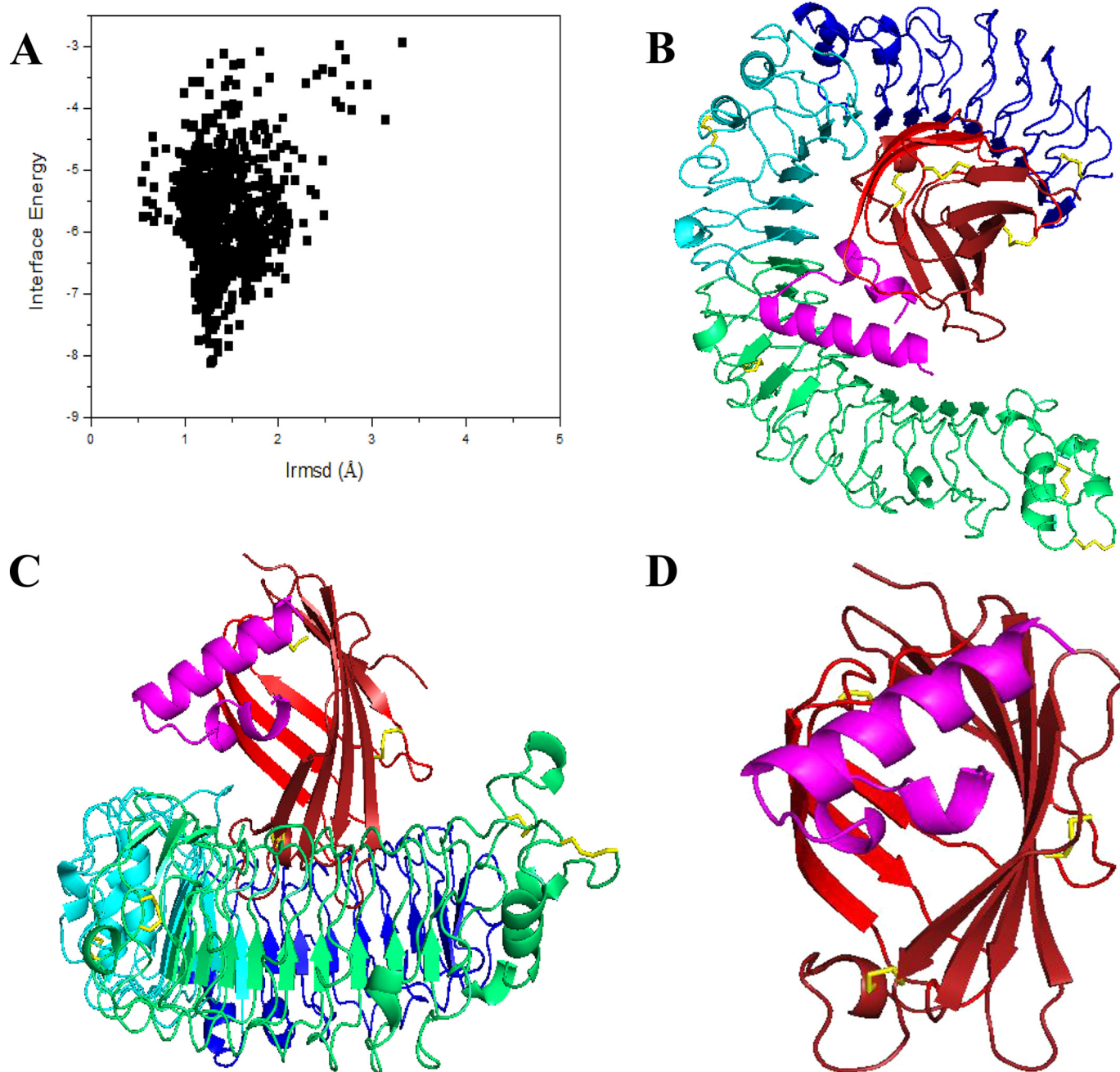


FIGURE 12. **Molecular docking structure of Hc-CATH with TLR4/MD2 complex.** *A*, 1000 decoy structures from a flexible docking study of TLR4/MD2 peptide by RosettaDock. The *horizontal axis* represents the root mean square deviation value compared with the initial structure during flexible docking, whereas the *vertical axis* represents the interface binding energy score of RosettaDock. *B*, overall structure of Hc-CATH binding with the TLR4/MD2 complex from a vertical angle. The N-terminal, central, and C-terminal domains of TLR4 are shown in *blue, cyan, and green*, respectively. The  $\beta$ -strands of MD2 are shown in *red*. The disulfide bridges are shown in *yellow* and Hc-CATH in *magenta*. *C*, overall structure of Hc-CATH binding with the TLR4/MD2 complex from a horizontal angle. *D*, elaborate structure of Hc-CATH binding with MD2.

the cathelicidin family AMPs have been well studied (21–23). The defensins are simply predicted from snake genomes by bioinformatic analysis, and their exact structures and functions remain unknown (38). Besides cathelicidins and defensins, the other AMPs identified from snakes include omwaprins (39) and crotamines (40). As a special kind of snakes living in the ocean, sea snakes inhabit a completely different ecological niche and encounter distinct pathogens compared with terrestrial snakes. Some sea snakes even have been found in rivers and freshwater lakes in Thailand, Cambodia, the Philippines, and Rennell

Island in the Solomon archipelago, which implies that they have evolved a more powerful immune system that enable them to resist pathogens from both land and ocean. However, little information is available on the immune system of sea snakes, and to our knowledge, no AMP has been identified from them thus far.

In our work, a novel cathelicidin family AMP, which we named Hc-CATH, was successfully identified from the venom gland of sea snake *H. cyanocinctus*. The cDNA encoding the Hc-CATH precursor is composed of 732 base pairs, and the

## The First Cathelicidin from Sea Snakes

translated Hc-CATH precursor comprises 187 amino acid residues (Fig. 1A). By multi-sequence alignment, we found that the Hc-CATH precursor shares a similar primary structure with other vertebrate cathelicidins, including an N-terminal signal peptide sequence, a middle cathelin domain, and a C-terminal mature peptide (Fig. 2). According to previous studies on snake cathelicidins (22), the Hc-CATH mature peptide was predicted as KFFKRLKSVRRRAVKKFRKKPRLIGLSTLL. Hc-CATH is composed of 30 amino acids and is highly positively charged, possessing a net charge of +12 (Table 1). Hc-CATH exhibits low sequence similarity with other cathelicidins, and it shows the highest similarity (60%) with cathelicidin-OH from the king cobra (23). To confirm the existence of native Hc-CATH in snakes, we prepared a polyclonal antibody of Hc-CATH and performed Western blot analysis. We identified the apparent expression of Hc-CATH in the snake venom gland, spleen, lung, and skin (Fig. 1B), consistent with the current concept that cathelicidins are expressed mainly in epithelial tissues and immunocytes (13, 16, 17). However, we did not observe the expression of Hc-CATH in muscle. This may be because the expression level in muscle was extremely low and could not be detected by Western blot. Furthermore, we studied the secondary structure of Hc-CATH using both a bioinformatics method and circular dichroism spectroscopy. Hc-CATH mainly assumes a typical amphipathic  $\alpha$ -helical conformation, with the hydrophobic amino acids concentrating on one side of the helix and the hydrophilic cationic amino acids on the other, which is universal for cationic linear AMPs (Fig. 4). Cationic AMP-mediated bacterial killing generally can be divided into several steps. First, AMPs are attracted to bacterial surfaces by electrostatic bonding between cationic peptides and anionic bacterial surface structures, such as anionic phospholipids, LPS in Gram-negative bacteria, and lipoteichoic acid in Gram-positive bacteria (10). Once close to the bacterial surface, the peptides can interact with lipid bilayers, adsorbing and embedding into the lipid head groups. As the number of bonding peptides increases, they begin to change their orientation from parallel to the bacterial membrane to perpendicular to the membrane, which ultimately results in the formation of transmembrane pores and the death of bacterial cells. The amino acid composition, amphipathicity, and cationic charge significantly influence the antimicrobial efficiency of AMPs (10). Accordingly, the highly positive charge and the typical amphipathic  $\alpha$ -helical conformation of Hc-CATH may be responsible for its potent antimicrobial activity.

Traditionally, sea snakes and terrestrial elapid snakes were believed to originate from the common elapid ancestors (41). However, the taxonomic status of sea snakes is still under review. At least three completely different taxonomic hypotheses exist, with recent research supporting the concept that Laticaudinae (sea kraits) and Hydrophiinae (true sea snakes) evolved from different ancient terrestrial elapids. It was proposed that sea kraits are closest to some Asiatic elapids, and true sea snakes exhibit a closer relationship with Australian elapids (42). Cathelicidins have been highly conserved in the long process of evolution, especially the N-terminal signal domain and cathelin domain (17). Phylogenetic analysis of cathelicidins provides valuable clues for the biological evolu-

tion study of vertebrates (28, 43). According to the phylogenetic tree constructed in the present study, all vertebrate cathelicidins clearly form five distinct clusters, in which Hc-CATH and other snake cathelicidins comprise a separate cluster (Fig. 3). This apparently indicates that sea snakes and other terrestrial snakes originate from a common ancestor. Additionally, we observed that Hc-CATH and PtCRAMP from the eastern brown snake, a typical Australian elapid, comprise a separate subcluster supported by a bootstrap value of 73% (Fig. 3). The close relationship between Hc-CATH and PtCRAMP provides evidence supporting the hypothesis that true sea snakes originated from ancient Australian elapids (42).

We further examined the antimicrobial potency of Hc-CATH using a standard 2-fold broth microdilution method. Hc-CATH exhibited potent and broad-spectrum antimicrobial activity against a variety of human pathogenic microorganisms (MICs ranging from 0.16 to 20.67  $\mu\text{M}$ ), of which most are ampicillin-resistant (Table 3). Unlike our previously characterized cathelicidin-BF from *B. fasciatus* (22) and viperidins from the South American pit viper, which are more active against Gram-negative bacteria as shown in a report by Falcao *et al.* (21), Hc-CATH showed a relatively equivalent activity against both Gram-negative and Gram-positive bacteria. This is consistent with the complex living environment of the sea snake *H. cyanocinctus* and the diverse pathogens they may encounter. Besides human pathogenic microorganisms, we also examined the antimicrobial effect of Hc-CATH toward marine aquatic pathogens. Hc-CATH displayed potent antimicrobial activity against all of the tested marine aquatic bacteria (Table 3). These bacteria are important pathogens that usually can be isolated from marine reptiles with severe infections. Therefore, the results indicate that Hc-CATH, synthesized primarily in snake epithelial tissues and immunocytes, plays important roles in host defense against pathogenic invasions. To investigate the effect of the  $\alpha$ -helical conformation and the positive charge on the antimicrobial and anti-inflammatory activity of Hc-CATH, we designed two Hc-CATH derivatives, Hc-CATH1 and -2 (with a decreasing positive charge but remaining in the  $\alpha$ -helix conformation) and an isotype control peptide, sHc-CATH (still having a positive charge identical to that of Hc-CATH but without the  $\alpha$ -helix conformation). Consistent with our speculation, the three peptides exhibited decreased antimicrobial and anti-inflammatory activities (Table 4 and Figs. 7C and 8G), which emphasizes the importance of the  $\alpha$ -helix conformation and positive charge on the activities of Hc-CATH. Disruption of the fixed amphipathic  $\alpha$ -helical structure resulted in the complete loss of antimicrobial and anti-inflammatory activity. Similarly, reducing the positive charge of Hc-CATH significantly decreased the antimicrobial and anti-inflammatory activity. Furthermore, compared with the positive control, meropenem, the bactericidal effect of Hc-CATH was more rapid. It killed the tested bacteria within 60 min (Table 5). This renders the bacteria unlikely to have evolved resistance toward Hc-CATH. Furthermore, Hc-CATH exhibited very low cytotoxicity toward mammalian cells, including tumor cell lines, normal cell line, primary mouse peritoneal macrophages, and human erythrocytes (Table 6). Besides, Hc-CATH was highly stable to salt, high temperature, solution, and serum protease degrada-

tion (Fig. 5), and Hc-CATH maintained the mainly  $\alpha$ -helix secondary structure in high salt solutions and at high temperatures (Fig. 4, E and F). All of the characteristics of Hc-CATH described above imply its promising therapeutic potential against microbial infections.

MST analysis indicated that Hc-CATH can bind directly to LPS (Fig. 10A), and an LPS neutralization assay indicated that the binding of Hc-CATH to LPS can neutralize the toxicity of LPS. Considering the secondary structure of positively charged Hc-CATH and the basic amino acid residues assembling on the defined hydrophilic side of amphipathic helix (Fig. 4, B and C), it can be rationally concluded that Hc-CATH binds to negatively charged LPS through direct electrostatic interaction. In fact, LPS neutralizing activity has also been characterized in several other cathelicidin peptides (28, 44). LPS is an important cell surface component of Gram-negative bacteria; therefore we speculated as to whether Hc-CATH can interact with Gram-negative bacteria. Flow cytometry analysis indicated that Hc-CATH bound to Gram-negative *E. coli* and Gram-positive *S. aureus* cells within 5 min (Fig. 6, A and B). Although there may be other components of the bacterial surface with which Hc-CATH can interact, the binding of Hc-CATH to bacterial cells should be the first step in Hc-CATH-induced bacterial death. SEM analysis clearly verified that treatment with Hc-CATH for 30 min induced the disruption of cytoplasmic membranes, leading to the lysis of the bacterial cells (Fig. 6, C–F), which is the exact antimicrobial mechanism of Hc-CATH.

The engagement of TLR4 by LPS triggers the activation of downstream signaling pathways, including MAPKs and NF- $\kappa$ B, leading to the production of pro-inflammatory cytokines involved in the pathophysiology of inflammation, sepsis, and other immune diseases (45). In this study, we found that Hc-CATH significantly inhibited the transcription and production of pro-inflammatory factors induced by LPS in mouse peritoneal macrophages, including NO, TNF- $\alpha$ , IL-1 $\beta$ , and IL-6 (Fig. 7 and 8). Especially, preincubation with Hc-CATH for 30 min achieved results similar to those found with the co-incubation group, which implies that unknown targets of Hc-CATH on the surface of the MPM cell membrane may be involved in the process of Hc-CATH-inhibited pro-inflammatory cytokine production. Furthermore, we used Western blot to investigate the mechanism of Hc-CATH-inhibited pro-inflammatory cytokine production. Hc-CATH markedly inhibited the LPS-induced phosphorylation of ERK, JNK, p38, and the translocation of NF- $\kappa$ B p65 subunit (Fig. 9). These results apparently indicate that Hc-CATH executes its anti-inflammatory effect through blocking the TLR4-mediated inflammatory response pathways induced by LPS. Besides LPS and bacterial cells (Figs. 10 and 11, A and B), Hc-CATH also can bind to MPM cells (Fig. 11C) and block TLR4 (Fig. 11D), indicating that TLR4 is a binding target of Hc-CATH on the surface of MPM cells. These results suggest that Hc-CATH simultaneously neutralizes LPS and blocks TLR4, inhibiting the binding of LPS to TLR4 and the activation of downstream signaling pathways, which ultimately decreases the production of pro-inflammatory cytokines. To understand the exact interaction mode of Hc-CATH and TLR4, we used a molecular docking method to predict the binding pattern involved in the interaction of the two molecules.

Because TLR4 and MD2 form a heterodimer receptor on the cell membrane that recognizes LPS, we therefore performed molecular docking of Hc-CATH and the TLR4/MD2 complex. To our surprise, the binding site of Hc-CATH was located at the entrance of the LPS-binding pocket in MD2 (Fig. 12). Therefore, we hypothesized that the binding of Hc-CATH to the TLR4/MD2 complex overlaps the LPS-binding pocket, which blocks the binding of LPS to MD2 and the activation of the downstream signaling pathways. Inflammation is a natural response of the innate immunity mounted to eradicate invading pathogens. However, an uncontrolled and overwhelming inflammation, such as “endotoxic shock” or septic shock, may cause severe injury to the host (6–8). The above results indicate that Hc-CATH serves as a pivotal modulator of sea snake innate immunity. It participates in the pathogen eradication process through direct antibacterial activity. Meanwhile, it prevents the occurrence of an excessive inflammatory response through its potent anti-inflammatory activity.

In conclusion, our study has described the identification and characterization of the first cathelicidin (Hc-CATH) from the sea snake *H. cyanocinctus*. Hc-CATH possesses potent, broad-spectrum, rapid, antimicrobial activity. It is highly stable and shows low cytotoxicity toward mammalian cells. It neutralized LPS, blocked TLR4, and exhibited strong anti-inflammatory activity. These properties make Hc-CATH a potent candidate for the development of peptide antibiotics.

## References

- Zasloff, M. (2002) Antimicrobial peptides of multicellular organisms. *Nature* **415**, 389–395
- Theuretzbacher, U., and Toney, J. H. (2006) Nature's clarion call of antibacterial resistance: are we listening? *Curr. Opin. Investig. Drugs* **7**, 158–166
- Spellberg, B., Powers, J. H., Brass, E. P., Miller, L. G., and Edwards, J. E., Jr. (2004) Trends in antimicrobial drug development: implications for the future. *Clin. Infect. Dis.* **38**, 1279–1286
- Akira, S., Uematsu, S., and Takeuchi, O. (2006) Pathogen recognition and innate immunity. *Cell* **124**, 783–801
- Tosi, M. F. (2005) Innate immune responses to infection. *J. Allergy Clin. Immunol.* **116**, 241–250
- Scott, M. G., Dullaghan, E., Mookherjee, N., Glavas, N., Waldbrook, M., Thompson, A., Wang, A., Lee, K., Doria, S., Hamill, P., Yu, J. J., Li, Y., Donini, O., Guarna, M. M., Finlay, B. B., North, J. R., and Hancock, R. E. (2007) An anti-infective peptide that selectively modulates the innate immune response. *Nat. Biotechnol.* **25**, 465–472
- Hancock, R. E., Nijnik, A., and Philpott, D. J. (2012) Modulating immunity as a therapy for bacterial infections. *Nat. Rev. Microbiol.* **10**, 243–254
- Finlay, B. B., and Hancock, R. E. (2004) Can innate immunity be enhanced to treat microbial infections? *Nat. Rev. Microbiol.* **2**, 497–504
- Radek, K., and Gallo, R. (2007) Antimicrobial peptides: natural effectors of the innate immune system. *Semin. Immunopathol.* **29**, 27–43
- Brogden, K. A. (2005) Antimicrobial peptides: pore formers or metabolic inhibitors in bacteria? *Nat. Rev. Microbiol.* **3**, 238–250
- Nakatsuji, T., and Gallo, R. L. (2012) Antimicrobial peptides: old molecules with new ideas. *J. Invest. Dermatol.* **132**, 887–895
- Zaiou, M. (2007) Multifunctional antimicrobial peptides: therapeutic targets in several human diseases. *J. Mol. Med.* **85**, 317–329
- Bals, R., and Wilson, J. M. (2003) Cathelicidins: a family of multifunctional antimicrobial peptides. *Cell. Mol. Life Sci.* **60**, 711–720
- Mookherjee, N., and Hancock, R. E. (2007) Cationic host defence peptides: innate immune regulatory peptides as a novel approach for treating infections. *Cell. Mol. Life Sci.* **64**, 922–933
- Ganz, T. (2003) Defensins: antimicrobial peptides of innate immunity.

## The First Cathelicidin from Sea Snakes

- Nat. Rev. Immunol.* **3**, 710–720
- Zanetti, M. (2004) Cathelicidins, multifunctional peptides of the innate immunity. *J. Leukoc. Biol.* **75**, 39–48
  - Zaiou, M., and Gallo, R. L. (2002) Cathelicidins, essential gene-encoded mammalian antibiotics. *J. Mol. Med.* **80**, 549–561
  - Mookherjee, N., Rehaume, L. M., and Hancock, R. E. (2007) Cathelicidins and functional analogues as antiseptics molecules. *Expert Opin. Ther. Targets* **11**, 993–1004
  - Chow, J. Y., Li, Z. J., Wu, W. K., and Cho, C. H. (2013) Cathelicidin a potential therapeutic peptide for gastrointestinal inflammation and cancer. *World J. Gastroenterol.* **19**, 2731–2735
  - Steinstraesser, L., Kraneburg, U., Jacobsen, F., and Al-Benna, S. (2011) Host defense peptides and their antimicrobial-immunomodulatory duality. *Immunobiology* **216**, 322–333
  - Falcao, C. B., de La Torre, B. G., Pérez-Peinado, C., Barron, A. E., Andreu, D., and Rádis-Baptista, G. (2014) Viperidins: a novel family of cathelicidin-related peptides from the venom gland of South American pit vipers. *Amino Acids* **46**, 2561–2571
  - Wang, Y., Hong, J., Liu, X., Yang, H., Liu, R., Wu, J., Wang, A., Lin, D., and Lai, R. (2008) Snake cathelicidin from *Bungarus fasciatus* is a potent peptide antibiotics. *PLoS One* **3**, e3217
  - Zhao, H., Gan, T. X., Liu, X. D., Jin, Y., Lee, W. H., Shen, J. H., and Zhang, Y. (2008) Identification and characterization of novel reptile cathelicidins from elapid snakes. *Peptides* **29**, 1685–1691
  - Wang, Y., Zhang, Z., Chen, L., Guang, H., Li, Z., Yang, H., Li, J., You, D., Yu, H., and Lai, R. (2011) Cathelicidin-BF, a snake cathelicidin-derived antimicrobial peptide, could be an excellent therapeutic agent for acne vulgaris. *PLoS One* **6**, e22120
  - Ling, G., Gao, J., Zhang, S., Xie, Z., Wei, L., Yu, H., and Wang, Y. (2014) Cathelicidins from the bullfrog *Rana catesbeiana* provides novel template for peptide antibiotic design. *PLoS One* **9**, e93216
  - Lu, Z., Wang, Y., Zhai, L., Che, Q., Wang, H., Du, S., Wang, D., Feng, F., Liu, J., Lai, R., and Yu, H. (2010) Novel cathelicidin-derived antimicrobial peptides from *Equus asinus*. *FEBS J.* **277**, 2329–2339
  - Zhang, X., Goncalves, R., and Mosser, D. M. (2008) The isolation and characterization of murine macrophages. *Curr. Protoc. Immunol.* Chapter 14, Unit 14.1
  - Wei, L., Yang, J., He, X., Mo, G., Hong, J., Yan, X., Lin, D., and Lai, R. (2013) Structure and function of a potent lipopolysaccharide-binding antimicrobial and anti-inflammatory peptide. *J. Med. Chem.* **56**, 3546–3556
  - Goldman, M. J., Anderson, G. M., Stolzenberg, E. D., Kari, U. P., Zasloff, M., and Wilson, J. M. (1997) Human  $\beta$ -defensin-1 is a salt-sensitive antibiotic in lung that is inactivated in cystic fibrosis. *Cell* **88**, 553–560
  - Travis, S. M., Anderson, N. N., Forsyth, W. R., Espiritu, C., Conway, B. D., Greenberg, E. P., McCray, P. B., Jr., Lehrer, R. I., Welsh, M. J., and Tack, B. F. (2000) Bactericidal activity of mammalian cathelicidin-derived peptides. *Infect. Immun.* **68**, 2748–2755
  - Berendsen, B. J., Elbers, I. J., and Stolker, A. A. (2011) Determination of the stability of antibiotics in matrix and reference solutions using a straightforward procedure applying mass spectrometric detection. *Food Addit. Contam. Part A Chem. Anal. Control Expo. Risk Assess.* **28**, 1657–1666
  - Okerman, L., Van Hende, J., and De Zutter, L. (2007) Stability of frozen stock solutions of  $\beta$ -lactam antibiotics, cephalosporins, tetracyclines, and quinolones used in antibiotic residue screening and antibiotic susceptibility testing. *Anal. Chim. Acta* **586**, 284–288
  - Pasupuleti, M., Schmidtchen, A., Chalupka, A., Ringstad, L., and Malmsten, M. (2009) End-tagging of ultra-short antimicrobial peptides by W/F stretches to facilitate bacterial killing. *PLoS One* **4**, e5285
  - Li, S. A., Lee, W. H., and Zhang, Y. (2012) Efficacy of OH-CATH30 and its analogs against drug-resistant bacteria *in vitro* and in mouse models. *Antimicrob. Agents Chemother.* **56**, 3309–3317
  - Ramanathan, B., Davis, E. G., Ross, C. R., and Blecha, F. (2002) Cathelicidins: microbicidal activity, mechanisms of action, and roles in innate immunity. *Microbes Infect.* **4**, 361–372
  - Kim, H. M., Park, B. S., Kim, J. I., Kim, S. E., Lee, J., Oh, S. C., Enkhbayar, P., Matsushima, N., Lee, H., Yoo, O. J., and Lee, J. O. (2007) Crystal structure of the TLR4-MD-2 complex with bound endotoxin antagonist eritoran. *Cell* **130**, 906–917
  - Viriyakosol, S., Tobias, P. S., Kitchens, R. L., and Kirkland, T. N. (2001) MD-2 binds to bacterial lipopolysaccharide. *J. Biol. Chem.* **276**, 38044–38051
  - van Hoek, M. L. (2014) Antimicrobial peptides in reptiles. *Pharmaceuticals* **7**, 723–753
  - Nair, D. G., Fry, B. G., Alewood, P., Kumar, P. P., and Kini, R. M. (2007) Antimicrobial activity of omwaprin, a new member of the waprin family of snake venom proteins. *Biochem. J.* **402**, 93–104
  - Oguiura, N., Boni-Mitake, M., and Rádis-Baptista, G. (2005) New view on crotamine, a small basic polypeptide myotoxin from South American rattlesnake venom. *Toxicon* **46**, 363–370
  - Sanders, K. L., Mumpuni, and Lee, M. S. (2010) Uncoupling ecological innovation and speciation in sea snakes (Elapidae, Hydrophiinae, Hydrophiini). *J. Evol. Biol.* **23**, 2685–2693
  - Sanders, K. L., Lee, M. S., Leys, R., Foster, R., and Keogh, J. S. (2008) Molecular phylogeny and divergence dates for Australasian elapids and sea snakes (hydrophiinae): evidence from seven genes for rapid evolutionary radiations. *J. Evol. Biol.* **21**, 682–695
  - Xiao, Y., Cai, Y., Bommineni, Y. R., Fernando, S. C., Prakash, O., Gilliland, S. E., and Zhang, G. (2006) Identification and functional characterization of three chicken cathelicidins with potent antimicrobial activity. *J. Biol. Chem.* **281**, 2858–2867
  - Xiao, Y., Herrera, A. I., Bommineni, Y. R., Soulages, J. L., Prakash, O., and Zhang, G. (2009) The central kink region of fowlcidin-2, an  $\alpha$ -helical host defense peptide, is critically involved in bacterial killing and endotoxin neutralization. *J. Innate Immun.* **1**, 268–280
  - Husebye, H., Halaas, Ø., Stenmark, H., Tunheim, G., Sandanger, Ø., Bogen, B., Brech, A., Latz, E., and Espevik, T. (2006) Endocytic pathways regulate Toll-like receptor 4 signaling and link innate and adaptive immunity. *EMBO J.* **25**, 683–692